10PW Short Pulse Laser Diagnostics

Contact *alexis.boyle@stfc.ac.uk*

Alexis Boyle
CLF,RAL

Marco Galimerti
CLF,RAL

Introduction

On the Vulcan facility, laser diagnostics are of paramount importance to ensure the correct performance of the laser and provide laser parameters to the user groups. Vulcan 10PW will require a more sophisticated version of the Vulcan diagnostics as the pulse length is much shorter, 30fs, with 300J of energy and a higher repetition rate, 10 minutes [1].

B-Integral

The B-integral through the back of the sample mirror (figure 3) is 12.2, calculated using equation 1[2], where λ is the central wavelength of the pulse and n_2 is the nonlinear refractive index of the propagation material.

$$B = \frac{2\pi}{\lambda}\int n_2 I(z)dz \qquad 1$$

Full Size Diagnostics

The full size diagnostics are mainly concerned with the spatial characteristics of the beam. After compression the beam is 600mm square and 30fs pulse length. Although the B integral is not critical for the integrity of the beam on these diagnostics, self focusing can cause issues with near field (NF) and far field (FF) measurements. We require the image plane of the 2nd grating to be relayed on to the NF diagnostics. Figure 2 shows the full size diagnostic channel is taken from a leak from the back of a mirror after the last grating in the compressor. An F3 parabola telescope will be used to collect the beam and reduce the beam size to 100mm square. As the leak from the sample mirror is expected to be about 1% and the beam is reduced by the 6:1 telescope the beam fluence will be about 0.04Jcm^{-2}. A glass dumper will be used to reduce the fluence to 0.0004Jcm^{-2}, shown in figure 3. The beam is then image relayed to the diagnostics table through a vacuum pipe.

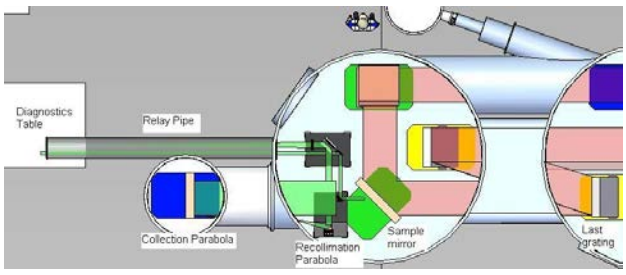

Figure 1: Sketch showing part of the compression chamber after the last grating, which houses the short pulse diagnostics channel.

Short Pulse Diagnostics

The B-integral through the back of the sample mirror will destroy any temporal information about the pulse. It is planned to take a sample of the beam through a hole drilled in the sample mirror. The energy in this line is expected to be 3-4J and the beam will be split into a high and low energy lines using a glass plate dumper, see figure 3. The high energy line will be for CW alignment and low energy operation. The low energy line will be for the on shot diagnostics. It is planned to deliver both high and low energy lines to the diagnostics table via the relay pipe under vacuum. The on shot energy line will have to be relayed using a parabolic mirror telescope, as the B-integral through lenses is greater than 1 which is still too high.

The short pulse diagnostics table will include spectral phase diagnostics, in the form of a single shot SPIDER, this device has been tested at the CLF [3] and a single shot autocorrelator. The contrast will be measured using a fast diode protected by a water cell, for the ns contrast and a single shot 3rd order cross correlator for the close in ps contrast. Spectrum, NF and FF pointing references will also be measured.

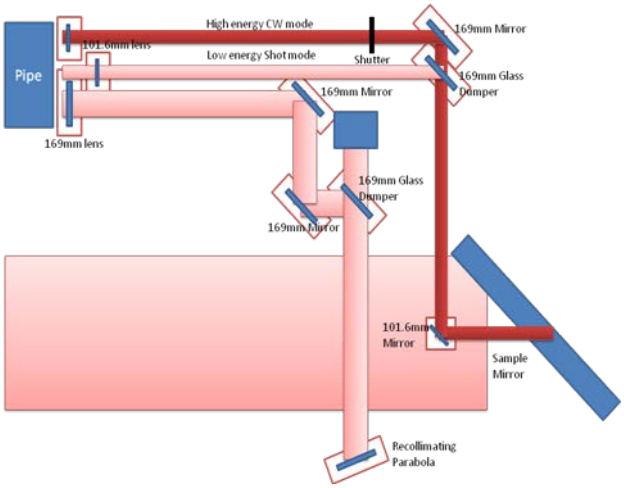

Figure 2: Sketch of the short pulse and full size diagnostics beam lines in the compressor chamber.

Diagnostics development

Devices such as the single shot spider and single shot 3rd order cross correlator are currently not used on the existing diagnostics on the Vulcan laser. It is planned to develop a single shot 3rd order device in the next year based upon other demonstrated devices [4].

Using the Vulcan laser as an example, it is planned to standardise the diagnostics, allowing for ease in component replacement, alignment and greater modularity. Standard beam heights, beam sizes and diagnostics components will be used as well as similar dumpers to deal with high energy operation. It is also planned to design devices that fit on 600mm x 300mm breadboards, allowing them to be slotted into bays.

Conclusions

In this article we present a possible layout for the short pulse diagnostics on the Vulcan 10PW laser. We also describe some of the issues that arise from trying to diagnose a high power, 300J, short pulse, 30fs pulse.

References

1. Vulcan 10PW TDR
2. A. E. Siegman, Lasers
3. Spider diagnostics techniques for Vulcan 10PW OPCPA project, M. Divoky, C. Hernandez-Gomez, p273-275 CLF Annual Report 2007-2008
4. High-dynamic-range single-shot cross-correlator based on a pulse replicator, C. Dorrer et al, University of Rochester LLE, Optics Express, Vol. 16, Issue 18, pp. 13534-13544 (2008)

Fighting Chromatic Aberration in 10PW

Contact *alexis.boyle@stfc.ac.uk*

Alexis Boyle
CLF, RAL

Marco Galimberti
CLF, RAL

Introduction

Future ultra short high power laser systems, such as the proposed the Vulcan 10PW upgrade, will require optical systems designed to handle growing bandwidth requirements of short pulses. The Vulcan 10PW laser is specified to operate 300J in 30fs and requires a bandwidth of 150nm centered at 910nm. To reduce the fluence of the laser, the beam propagation requires large aperture optics. In order to achieve best compression of the beam, the wavefront quality must be better than λ/10 peak to valley (P-V), across the bandwidth.

Layout and Description

The proposed optical system must propagate the laser beam from an intermediate stage at 28mm square clear aperture (CA) through 2 OPCPA (Optical Parametric Chirped Pulse Amplification) amplification stages, 200mm square CA, and be delivered to the compressor chamber at 600mm square CA.. Fig 1 shows the propagation through the OPCPA amplification stages, using lenses to expand and image relay the beam. There is an intermediate stage at 67mm square CA to reduce the power of the expanding vacuum spatial filters (VSF) and also include the addition of a deformable mirror for further wavefront correction. The VSFs are capped with fused silica lenses, unless specified.

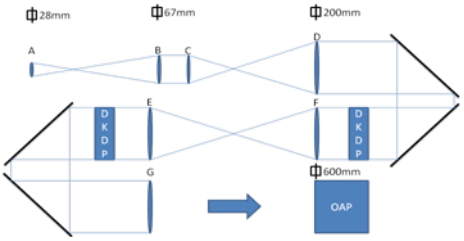

Fig 1: Simplified layout of the beam propagation system through the OPCPA amplification stages. Letters A to G denote lens positions.

The modeling of the optical systems was done using Zemax [1]. The wavefront quality was controlled by optimising the beam divergence at the input faces of the two DKDP crystals and at the output of the optical system. The beam was sampled at equally spaced points across the pupil and at 5 wave bands over 170nm bandwidth centered at 910nm, this was to guarantee performance over 150nm bandwidth. It should be noted that the choice of glass types is fairly limited at large aperture [2].

Ghosting

Ghosting is caused by multiple reflections from surfaces propagating through the system causing unexpected foci that might damage optics. Although reflections can be minimised using thin film coatings, propagating ghost energy can be as high as 4J. A simple spreadsheet was created for each solution to calculate the positions of ghost foci from to 3 reflections. If the position of foci were in or near to any optic, Zemax was used to calculate the size of the focal spot to ascertain any possible impact.

Doublet Solution

Referring to fig. 1, there are identical fused silica CaF2 doublets at D, E and F, the VSF between the two DKDP crystals is symmetrical. There is a F2 fused silica doublet at position G. Fig. 2 shows the optical path difference (OPD) plot across the pupil. The maximum chromatic aberration between 825nm and 995nm is λ/10, so over the 150nm bandwidth <λ/10. Higher order spherical is the predominant aberration due to the spherical nature of the lenses. The collimation at both crystal surfaces was 0.05mrad. It is important that the wavefront at the crystal is as flat as possible for the phase matching in the OPCPA amplification.

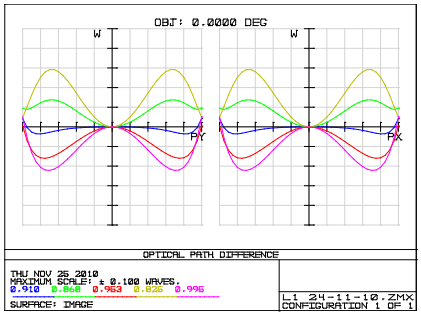

Fig 2: Zemax OPD across the pupil at the output of the optical system for the doublet solution over 170nm.

Mixed Lens and Parabola Solution

Referring to fig. 1 there are aspheric fused silica lens and off axis parabolas (OAPs) at positions D and F to recollimate the beam. The VSF lenses at B and E are BK7. Fig. 3 shows the chromatic aberration to be better than <λ/50, which is diffraction limited and the beam divergence of 0.0004mrad on the crystal surfaces over 300nm. Higher order spherical aberration is visible, due to the spherical nature of the lenses.

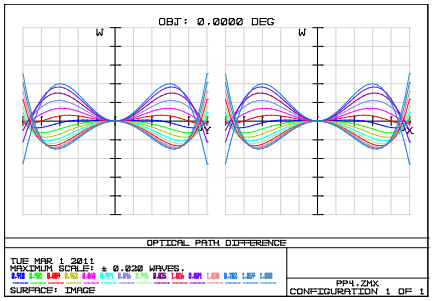

Fig 3: Zemax OPD across the pupil at the output of the optical system for the parabola solution over 300nm.

Conclusions

Here we have modeled two different approaches for an optical system to propagate a 150nm chirped pulse through large aperture OPCPA amplification stages. Both systems fulfill wavefront requirements for the propagation through the DKDP crystals and delivery to the compressor. The doublet system shows a good performance, <λ/10 over 150nm, with low beam divergence, 0.05mrad, at the crystal surfaces. The parabola solution is diffraction limited. Both exhibit higher order spherical aberration.

References

1. Zemax lens design software, Radiant ZEMAX LLC, www.zemax.com.
2. Schott glass availability and private communication with HVSkan (Schott representatives in UK)

10PW compressor requirement analysis

Contact *marco.galimberti@stfc.ac.uk*

M. Galimberti, S. Blake, S. Hancock, C. Hernandez-Gomez, I. Musgrave, I. Ross, T. Winstone

Central Laser Facility, Science and Technology Facilities Council
Rutherford Appleton Laboratory, Harwell Science and Innovation Campus, Didcot, OX11 0QX

Introduction

The 10PW project requires to be able to provide laser pulses shorter than 30fs[1]. To enable the design of the compressor and the amplification chain it is crucial to define the stability requirement for the optics and the alignment. It is also important to understand which parameters will have an impact on the pulse length and, more in general, on the final specification of the facility.

Spectral shape

It is important to ensure that the 30 fs specification can be met using the OPCPA amplification architecture chosen. The broadband seed generated in the Front End will have a 150nm bandwidth, 1 J of energy. In the large OPCPA amplification stages the pulse needs to be amplified further to 500 J whilst preserving all the bandwidth, this is critical to achieve a short pulse.

There are several important parameters that will dictate what the final pulse length will be. These key parameters are: pulse bandwidth and spectral shape, stretcher and compressor design, chromatic aberration, wavefront, grating surface quality, the B integral and alignment errors.

The stretched pulse length has been set to 3 ns with a 150nm of bandwidth. The spectral shape of the pulse prior to compression is critical in the compression process. Two different spectral shapes were considered as shown in fig. 1. The first one has a square temporal profile, labeled as "*full*", and uses all the available bandwidth while the second one, labeled "optimal" ("*opt*"), has a smaller FWHM but still using the same spectral region.

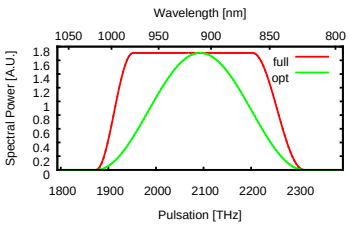

Figure 1: Spectral pulse shapes

The spectral shape of the second pulse was generated in order to minimize the second momentum in time σ, defined as:

$$\sigma^2 = \frac{\int t^2 I(t)\,dt}{\int I(t)\,dt}$$

where *I(t)* is the intensity of the pulse at time *t*, forcing the spectrum of the pulse to remain in the available bandwidth. The pulselength obtained with this spectral shape is shown in fig. 2 left and compared to the pulse obtained by using the 'full bandwidth shape'. The optimum case represents the shortest available pulse characterised by a smaller bandwidth at FWHM compared to the full bandwidth at FWHM. It can be seen that the increase to the pulse length at FWHM is minimal.

The spectral shape however has a big impact in the overall contrast, as shown in fig. 2 right.

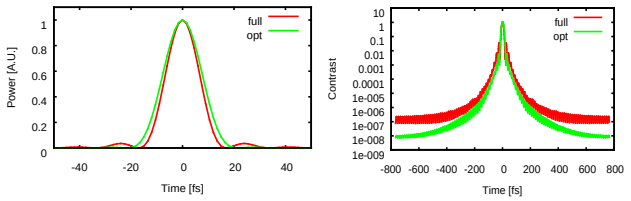

Figure 2: Pulselength for full bandwidth and optimum bandwidth cases (left); Contrast for full bandwidth and optimum bandwidth cases (right).

Compressor

The planned compressor for the 10PW project is composed of 4 gratings in an off plane geometry. The gratings are planned to work in Littrow with a off plane angle. For the simulation presented in this report the following parameters have been used: off plane angle of γ=17°, line density 900 mm^{-1}, distance between the gratings of D=3360 mm, gratings size 80cm x 115.5cm.

Simple Compressor Simulation

The impact on pulse length by the different key factors for the two cases has been modeled. The numerical code is based on a ray tracer able to simulate the compressor. Each of the parameters taken into account has been studied separately, extracting the dependency of the pulse length. The final pulse length has been obtained supposing total decoupling between the parameters and summing in quadrature each single contributions. The results are shown in table 1.

Optimal			*Limit*	*Contr. [fs]*	*FWHM [fs]*
Pulse					17.6
Gratings	Angular	Rot [μrad]	4	9.0	
		Tip [μrad]	8	8.6	
		Tilt [μrad]	4	9.3	
	Surface	1/λref	8	6.5	
	Distance [μm]		10	4.8	
	Sub Total				17.5
Beam	Pointing [μrad]		100	0.1	
	Front	1/λ0	10	0.8	
	Chromatic	1/λ0	10	5.6	
	Sub Total				5.6
Phase	Bint		0.5	5.7	
	Phase [rad]		0.1	2.5	
	Sub Total				6.3
Final					26.3

Full Bandwidth			*Limit*	*Contr. [fs]*	*FWHM [fs]*	*FWHM via σ [fs]*
Pulse					14.7	22.2
Gratings	Angular	Rot [μrad]	3	7.9		
		Tip [μrad]	7	9.1		
		Tilt [μrad]	3	9.8		
	Surface	1/λref	8	8.6		
	Distance [μm]		10	7.0		
	Sub Total				19.1	
Beam	Pointing [μrad]		100	0.2		
	Front	1/λ0	10	2.4		
	Chromatic	1/λ0	10	6.9		
	Sub Total				7.3	
Phase	Bint		0.5	8.6		
	Phase [rad]		0.1	3.7		
	Sub Total				9.4	
Final					26.9	31.6

Table 1: "Optimal" bandwidth pulse length case (left); "Full" bandwidth pulse length case (right).

A contribution to the pulse length increase is due to the compressor gratings. Alignment errors in the compressor and misalignments between the stretcher and compressor will contribute to an increase in pulse length. The tolerances of grating parallelism and groove parallelism have been to minimise the contribution to the pulselength. The tolerances for the tilt, tip and rotation for each grating has been analysed. Looking at the compressor as a whole, the tolerances in the angular motions have been set to 4 micro-radians for tilt and rotation and 8 micro-radians for tip, for the "optimal" case, and to 3 micro-radians for tilt and rotation and 7 micro-radians for tip, for the "full" bandwidth case. While the tolerance grating distance is set to 10 microns. We also need to take into account

possible wavefront errors coming from the grating surface as this also contribute to the overall pulse length. Grating surface quality has been set to be λ /8.

Other important aspects that will affect the pulse length are the pulse wavefront quality, chromatic aberration and input angle of the pulse entering the compressor. With large bandwidths chromatic aberration is of high importance, all optics expanding the beam up to the input of the compressor will be designed to minimize the chromatic errors. In addition the input beam wavefront may be affected by the quality of optical components such as crystals; all these static wavefront errors could be corrected if necessary by using adaptive optics. The overall wavefront quality entering the compressor has been set to be λ /10 or better. If these requirements are met the pointing and wavefront errors will add to the pulse length as shown in table 1. The contribution to the pulse length from B integral, expected to be 0.5 rad, has also been calculated to be respectively 5.7 fs and 8.6 fs.

Finally, taking all these key factors in to consideration our model predicts a 26.3 fs pulse for the "optimal" case while for the "full" bandwidth case two values are predicted: 26.9 fs and 31.6 fs. The difference is dependent on how each contribution are summed. For the "optimal" case, summing in quadrature the FWHM of the pulse and the σ within the different contributions provide the same value. However, for the "full" bandwidth case, FWHM and the σ are quite different, obtaining two final values.

Corner Montecarlo Simulation

While the model used is able to provide the required limits for the design of the compressor and the amplification chain, a more detail simulation is required to investigate in more detail the pulse length, in particular on the expected focal spot.

On the other hand, because the case of "full" bandwidth will be able to provide higher energy but it appears to be more critical, better understanding of the contribution of the parameters is definitely useful.

To that purpose, a corner Montecarlo simulation has been performed. For a set of parameters, the compression and focusing (as planned for TAP10) of a pulse has been simulated. The parameters have been selected randomly to be plus or minus the limit, i.e. only two values for each parameter were allowed. Only the "full" bandwidth case has been considered.

The energy before compression has been fixed to 500J while the efficiency of the gratings has been fixed to 90% each. The results, are based on over near 13000 run, are shown in the fig. 3.

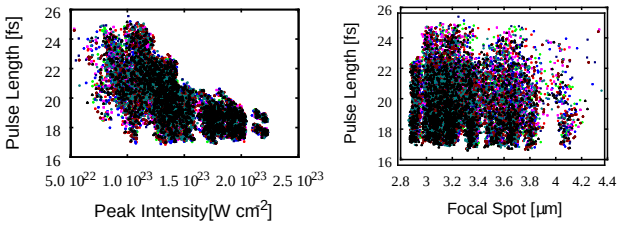

Figure 3: Montecarlo results.

The expected pulse length in the focal spot is between 17fs and 26fs, within a spot size (w) between 2.9 μm and 4.4 μm. The peak intensity is expected to be between $5 \cdot 10^{22}$ W·cm^{-2} and $2.2 \cdot 10^{23}$ W·cm^{-2}, while the energy in the focal spot (2w) will be between 250J and 330J. The "corner" values, i.e. the best and the worst obtained in the runs, are summarized on tab. 2.

FWHM [fs]					
File	**pos**	**min**	**File**	**pos**	**max**
Ris_1	984	16.9	Ris_5	1556	25.6
Peak Intensity [W cm^{-2}]					
File	**pos**	**min**	**File**	**pos**	**max**
Ris_6	251	5.3 10^{22}	Ris_2	192	2.2 10^{23}
Spot [μm]					
File	**pos**	**min**	**File**	**pos**	**max**
Ris_3	1314	2.9	Ris_7	796	4.4
Energy 2w [J]					
File	**pos**	**min**	**File**	**pos**	**max**
Ris_6	1121	247	Ris_3	1208	332

Table 2: Corner result summary from the Montecarlo simulation.

Analyzing in more detail the corner cases (fig. 4), the pulse shape is expected to change with case to case, showing in same case the presence of a shoulder, pre or post pulse (fig. 5 left). The focal spot shows wings in two cases, affecting the peak intensity. The results also show some pulse front tilt in the dispersion plane.

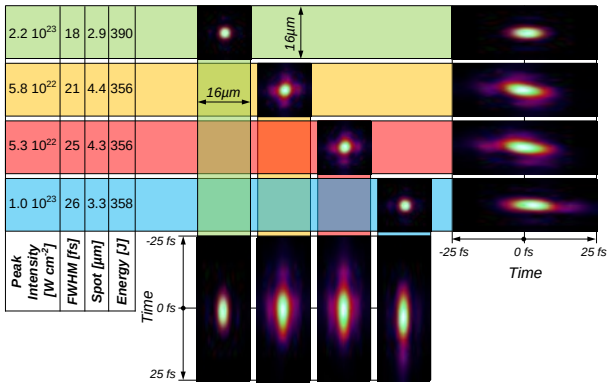

Figure 4: Expected pulses in the focal spot.

Finally, the close contrast of the pulse will not be affected, as shown in fig. 5 right. To be notice that intensity below 10^{11} W cm^{-2} are affected to numerical errors.

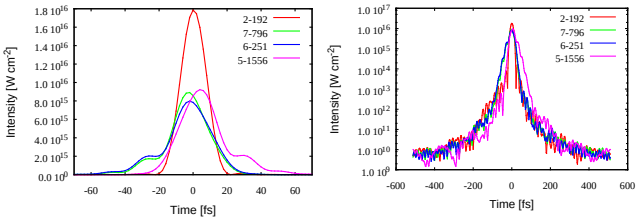

Figure 5: Expected pulse shapes in the focal spot (left) and expected close contrast (right).

Conclusions

The compression of the expected 10PW pulse has been simulated taking into account different realistic parameters. From a simple model a set of parameter requirement for the optical mount and beam quality has been produced.

A more realistic simulation confirms the requirement of the simple model. The final results show pulse length less than 26fs, below the required 30fs, with a peak intensity greater than $5 \cdot 10^{22}$ W·cm^{-2}.

References

1. *"The Vulcan 10PW Project: Facility Design Report"*, Central Laser Facility, STFC, RAL, October 2010

Influence of the deuteration level on DKDP OPCPA amplifier

Contact *marco.galimberti@stfc.ac.uk*

M. Galimberti, C. Hernandez-Gomez, I. Musgrave, I. Ross, T. Winstone

Central Laser Facility, Science and Technology Facilities Council
Rutherford Appleton Laboratory, Harwell Science and Innovation Campus, Didcot, OX11 0QX

Introduction

To deliver the energy requirement for the Vulcan 10 PW facility, 300J in 30fs, the broadband seed laser pulse generated by the front end, 150nm bandwidth centered on 910nm, needs to be amplified before it is injected into the compressor [1]. The pulse energy needs to be increased from 1J, at the output of the front end, to the required 500J prior to the compressor. It is also important to preserve the bandwidth of the pulse during the amplification. The amplification scheme selected is based on the *Optical Parametric Chirped Pulse Amplification* (OPCPA) technique: a *Optical Parametric Amplification* (OPA)[2] scheme where the Signal beam is a chirped pulse.

Suitable media for OPCPA are second order nonlinear crystals, like LBO, BBO, KDP, DKDP, etc. Because the energy required at the output is 500J, this limits the type of crystal. While the size of the beam is limited by the damage threshold of the optics, the size of the crystal must be of the order of 200mm square. The only commercially available crystals of this size are KDP and DKDP, where the difference between the two is the substitution of the hydrogen with deuterium. The amount of deuteration changes the optical properties on the crystals and it has impact also in the cost. It is important to study its impact on the performance of the planned amplification scheme.

Optical Parametric Amplification

The energy is provided by a laser pulse, called *Pump*, with a wavelength λ_P and intensity I_P. This beam is injected into a specific nonlinear medium together with the laser pulse that is required to be amplified, called *Signal* and having a wavelength λ_S and intensity I_S. If the intensity of the pump beam is higher than the signal beam and if $\lambda_P<\lambda_S$, it is possible to amplify the signal taking power from the pump. Meanwhile, in the process a third beam is created, called Idler, and with a wavelength λ_I equal to

$$\frac{1}{\lambda_I}=\frac{1}{\lambda_P}-\frac{1}{\lambda_S} \qquad \textit{Equation 1}$$

To have an appreciable transfer of power it is also required that the refractive indexes of the medium at the three different wavelengths must be close. More precisely, if $\vec{k}_P$, $\vec{k}_S$ and $\vec{k}_I$ are the wave vectors for, respectively, the Pump, Signal and Idler beams, the equation $\vec{k}_P=\vec{k}_S+\vec{k}_I+\vec{dk}$ must be satisfied (see fig. 1) where $\vec{dk}$ must be small compared to the length of the medium L_C: $dk \cdot L_C \lesssim 2\pi$. Ideally it should be $dk=0$. That condition is known as *phase matching*. $\overrightarrow{OA}$ is the optical axis of the medium, θ is called the *phase matching angle* and α_P is called the *non-collinear angle*.

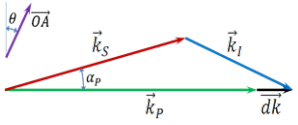

Figure 1: Vectorial equation for the phase matching.

To achieve the phase matching condition, the birefringence of the crystals is used. Taking into account only uniaxial crystals, the Signal is sent inside as an ordinary wave while the Pump beam will be an extraordinary wave. In this way the phase matching could be tuned by changing the angle of the pump beam with respect to the optical axis. This scheme to obtain the phase matching is called Type I.

Analyzing the refractive index for the two crystals KDP and DKDP, selecting a pump beam at λ_P=526.5 nm and scanning different non-collinear angle, it is possible to find a configuration for the DKDP where the phase matching condition is satisfied over a bandwidth more than 150nm around the central wavelength of 910 nm.

Phase matching and deuteration level

The DKDP crystal meets the requirements for the amplification bandwidth and available size, however the deuteration level is a key parameter that requires further investigation. DKDP is the deuterated version of the KDP. There are few differences between KDP and DKDP but they are quite important for our application: the absorption is different in the IR region and the phase matching curves are slightly different [3]. The difference in the phase matching means that the KDP does not show the same big bandwidth at 910nm. Meanwhile, the absorption in the IR could affect the Idler, which will be in the region between 1140 nm and 1420 nm (fig. 2).

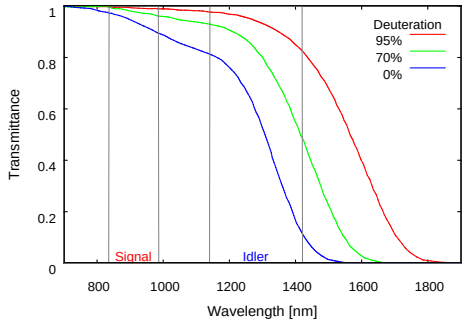

Figure 2: Internal transmittance of DKDP for different deuteration level

The changes in the absorption and the refractive index between the two crystals are connected to the group OH. Replacing the hydrogen with deuterium affects both absorption and phase matching. The level of the substitution could change. There are commercially available DKDP crystals with different deuteration levels. Usual values are 70% and 95%. While higher deuteration level will be better for the absorption and the bandwidth, the difference in price between the two levels is quite significant.

To study the effects of the deuteration level a numerical code has been used. The code is able to simulate the OPCPA amplification taking into account the different deuteration level, phase matching, saturation effects and absorption in the crystal.

A single crystal 50mm long was considered, looking at the small signal gain in the spectral region between 810 nm and 1050 nm. The intensity of the pump was fixed at 6.4 10^8 Wcm^{-2}. For different deuteration levels the two angles θ and α_P were selected to maximize the gain over a bandwidth of 150 nm

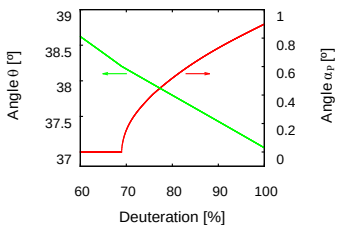

Figure 3: Optimum non collinear angle angles α_P and phase matching angle θ for different deuteration level.

around 910 nm. The results are shown in fig. 3. Around 68% of deuteration there is a clear change of behaviors, where the optimal α_P starts to be different from 0.

Looking at the small signal gain for different wavelengths, as shown in fig. 4, the deuteration level affects the blue region of the spectrum, shifting the left edge to longer wavelength while the deuteration ratio decreases. For a value less than 68%, the shift will become more important. On the rest of the spectrum, the gain remains quite uniform over all the bandwidth. The right edge is shifting faster than the left one. This is primarily connected with the change of the phase matching. In order to obtain gain over all the required bandwidth for a lower deuteration level, it is required to move close to the degenerate case, where the signal and the idler have the same wavelength. Even if in this case the bandwidth could be quite wide, having the idler in the same spectral region as the signal could badly affect the contrast and stimulate parametric emission from the crystal.

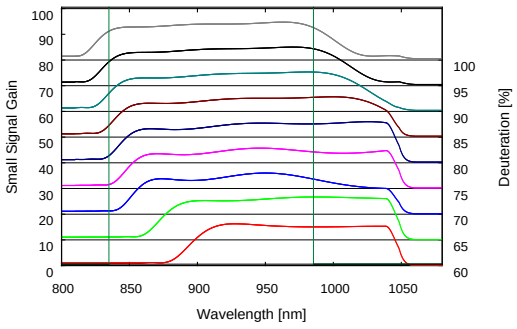

Figure 4: Spectral small signal gain for different deuteration levels. Each curve has been shifted for clarity. The two green vertical lines indicate the spectral region of the signal, 150 nm around 910 nm.

The simulation shows that any deuteration above 70% is appropriate and would satisfy the amplification requirements. However, taking into account the accuracy of the crystal deuteration level that can be achieved during the growing process, a value around or greater of 80% is more may be advisable to allow for errors in manufacturing.

Global system simulation

To investigate the thickness of the DKDP crystals required, the overall optical scheme has been simulated, with three stages and for 80% and 100% of deuteration level. The optical layout considered is shown in fig. 5. The signal laser pulse from the front end is defined to be 1J in a round beam about 40mm in. After that the beam will be apodized to a 28mm x 28mm square beam losing approximately 30% of energy, and then expanded up to 200mm x 200mm. The size of the beam has been fixed to keep the fluence of the pump beam around 1.5Jcm^{-2} to avoid damage in the optics and ensure an appropriate operational life.

The pump beam pulse is 3ns long at 526.5nm while the signal pulse is a stretched pulse of 3ns and 150nm of bandwidth centered at 910nm. Both pulses are assumed to be rectangular in time. The signal chirp was supposed linear. The crystal lengths were found optimizing the energies after each stage.

The losses of the different optical components were taken into account. In particular the crystals were supposed to be AR coated with a reflectivity of 0.25% for the signal and 1% for the pump. The green mirrors before and after the crystals are

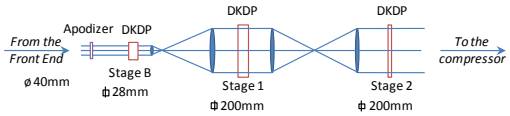

Figure 5: Simulated optical layout.

assumed to have a transmittivity of 97% while an efficiency of 96% is assumed for the VSFs (Vacuum Spatial Filter).

The results of the simulations are summarized in table 1. The energies shown are considered inside the crystals, except for the input and the output. The efficiency is the ratio between the energy transferred to the signal and the energy lost by the pump. The absorption is calculated by balancing the energies in the process.

			Front End	Stage B	Stage 1	Stage 2	Output	Stage B	Stage 1	Stage 2	Output
Deuteration				80%				100%			
θ [°]				38.4				38.0			
α_P [°]				0.52				0.90			
Crystal Length [mm]				63.8	82.6	33.2		64.6	82.6	33.3	
Small Signal Gain				88.6	485	5.9		87.8	445	5.6	
IN	Signal	Energy [J]		0.59	5.9	271		0.59	6.4	299	
		λ_{min}[nm]		835	842	846		835	837	839	
		λ_{max}[nm]		985	985	983		985	984	982	
		$\Delta\lambda$[nm]		150	143	137		150	147	143	
	Pump	Energy [J]		12	594	595		12	594	595	
OUT	Signal	Energy [J]	1	6.59	302	576	530	7.12	333	629	579
		λ_{min}[nm]	835	842	846	845	845	837	839	839	839
		λ_{max}[nm]	985	985	983	983	983	984	982	983	983
		$\Delta\lambda$[nm]	150	143	137	138	138	147	143	144	144
	Pump	Energy [J]		1.2	74	55.6		0.4	30	23.4	
	Idler	Energy [J]		3.34	164	177		3.81	190	196	
		λ_{min}[nm]		1140	1140	1140		1140	1140	1140	
		λ_{max}[nm]		1400	1390	1400		1420	1420	1420	
Efficiency				51%	50%	51%		56%	55%	56%	
Absorption				10%	10%	7%		8%	8%	5%	

Table 1: Simulated energies and spectra for the three stages option at 80% and 100% deuteration level.

The lengths of the crystal are almost the same for the two deuteration levels modeled. As already discussed above, reducing the deuteration level shifts the lower wavelength of the signal to the red region. In this case the shift is 5nm, thus reducing the final bandwidth by 5nm.

In term of energies, using 80% of deuteration implies losses approximately 2% of energy compared to the 100% case while moving from two to three stages improve the final energy of about 1-2%. The expected efficiency is always around or more than 50%. The total absorption in the crystals is expected to be between 5% and 10%.

Conclusions

The influence of the deuteration level of the DKDP in the planned amplification stages of the 10PW project has been modeled. While a deuteration level of 100% will provide better results in term of bandwidth and efficiency, a level bigger than 80% could be used with degrading the specification of the project.

References

1. *"The Vulcan 10PW Project: Facility Design Report"*, Central Laser Facility, STFC, RAL, October 2010
2. **R. A. Byer and R. L. Baumgartner,** "Optical Parametric Amplification". *IEEE Journal of Quantum Electronics.* 1979, Vols. QE-15, 6, pp. 432-444.
3. **T. R. Sliker, S. R. Burlage.** Some dielectric and optical properties of KD2PO4. *Journal of Applied Physics.* 1963, Vol. 34, 7, pp. 1837-1840.

Study of Self Frequency Shifting Solitons in Photonic Crystal Fibre to generate a synchronised 1053nm for the 10PW Upgrade Project.

Contact *ian.musgrave@stfc.ac.uk*

Elizabeth Hemsley, Ian Musgrave and Andrey Lyachev

Central Laser Facility, STFC, Rutherford Appleton Laboratory, HSIC, Oxfordshire, OX 11 0QX, UK

Introduction

Included in the 10PW upgrade project for the Vulcan Laser is the provision for joint PW and 10PW operations in Target Area Petawatt. This will enable pump-probe experiments. For these type of experiments to be successful the pulses for the two beams to be synchronised with a relative jitter better than 200fs (FWHM). One way of achieving this is to use a common seed for both beam lines.

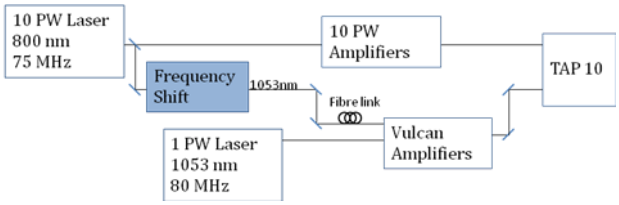

Fig 1: Schematic diagram of the upgraded Vulcan laser system.

The Vulcan laser is seeded at 1053nm, and the 10PW laser will be seeded at 900nm. Synchronization can be achieved by using a 10PW laser to seed the Vulcan amplifiers as shown in Fig1. However the 10PW pulse needs to be shifted to 1053nm before it can be amplified in Vulcan. The proposed method of this shift is to use an optical fibre, in which non-linear effects will change the frequency of the input light. Photonic crystal fibres (PCF's) are micro-structured fibres which can be engineered with highly non-linear properties [1]. Published experiments have used PCFs to produce many optical phenomena, such as supercontinua [2] and Raman shifted solitons [3,4].
This report outlines the effect of soliton self frequency shifting in fibres. A short length of fibre is then used experimentally with several different lasers in the 10PW front-end. By examining the output spectrums it is determined if the fibre is suitable for seeding the Vulcan laser.

Photonic Crystal fibres

Optical fibres consisting of a silica core surrounded by a periodic array of air holes are known as photonic crystal fibres. One example of an arrangement of holes can be seen in Fig 2. The microstructure of the fibre creates a photonic bandgap between the core and surrounding holes, which contains light in the core. Properties of the fibre, such as the zero dispersion wavelength and non-linearity, can be changed by varying the hole size and arrangement [5]. Custom made PCF's are useful for many different purposes, and can be designed to produce interesting phenomena in fibres.

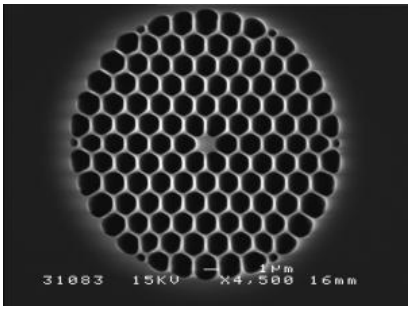

Fig 2: cross section of photonic crystal fibre. [6]

Nonlinear effects in fibres

A pulse of light propagating through a dielectric can be altered in a number of ways, due to the medium having a different response to varying parameters of light.
For example, group velocity dispersion (GVD) is caused by the wavelength dependent refractive index.
The medium is also behaves non-linearly at high intensities of light. The bound electrons in the medium have an anharmonic response to field strengths above a threshold power. This is the origin of the self phase modulation (SPM) effect in fibres, when using short powerful pulses. SPM also creates a chirp on the pulse.

It is useful to define the fibre length in terms of the dispersive length L_D and the non-linear length L_{NL}. These are the minimum fibre lengths needed for dispersive or non-linear effects to be visible.

$$L_D = \frac{T_0^2}{|\beta_2|}$$

$$L_{NL} = \frac{1}{\gamma P_0}$$

Where T_0 is the input pulse duration, β_2 is the group velocity dispersion parameter, P_o is the peak power, and γ is the nonlinear parameter.

Under certain circumstances the chirp and spectral broadening created by SPM can be counteracted by the GVD, if the wavelength is in the anomalous dispersion regime of the fibre. A self-sustaining pulse called a soliton is formed, which maintains its shape along the fibre when this happens. The soliton parameter N is given as;

$$N = \sqrt{\frac{L_D}{L_{NL}}}$$

If N=1 then a fundamental sech shaped soliton is formed, for N>1 the soliton's shape will periodically vary with length, but the central wavelength will remain the same.
The soliton can be perturbed during propagation, especially if the fibre is highly non-linear or the pulse length very short <1ps. One such perturbation is the soliton self frequency shift (SSFS). This is due to stimulated Raman scattering in the fibre, where the incident photon is inelastically scattered and transfers energy to vibrations of the SiO_2 bond, producing a phonon.
The overall effect of Intrapulse Raman Scattering (IRS) is to use the short wavelength parts of the pulse to pump the long wavelength parts, the overall effect is to red-shift the pulse during propagation.
Through a short fibre length, the frequency shift is approximately linear, and highly dependent on input pulse length;

$$\Omega \propto \frac{1}{T_0^4}$$

Over a longer distance a chirp develops due to group velocity dispersion, and the pulse length increases to compensate for changes in pulse energy. Eventually the Raman effect saturates, the pulse parameters reach an equilibrium, and the pulse is no longer red-shifted. The behaviour of the soliton over a length of fibre is governed by a set of coupled differential equations [7].

$$\Omega(z) = -\frac{8}{15}\gamma T_R T_0 P_0 \int_0^z \frac{e^{-\alpha z}}{T_p^3(z)} dz$$

$$\frac{dT_p}{dz} = \frac{\beta_2 C_p}{T_p}$$

$$\frac{dC_p}{dz} = \left(\frac{4}{\pi^2} + C_p^2\right)\frac{\beta_2}{T_p^2} + \frac{4}{\pi^2}\gamma P_0 e^{-\alpha z}\frac{T_0}{T_p} + \frac{12}{\pi^2}\beta_2\Omega^2$$

T_R is the Raman response time of the fibre, α is the attenuation in the fibre (can be neglected if small). T_P is the pulse length during propagation, which is dependent on C_p, the chirp. These equations can be solved numerically using the Runge-Kutta technique.

A supercontinuum is formed via many processes, and so is difficult to model. The soliton self frequency shift is the main process which transfers energy to longer wavelengths, and will be focused on in this report.

Experimental

This experiment uses a variety of laser pulses to investigate the non-linear and dispersive properties of a selected PCF, to determine if it is suitable to provide a 1053nm seed pulse for Vulcan.

Fibre Selection

The fibre NL-PM-750 was selected due to its high non-linear coefficient of 95 $(Wkm)^{-1}$, and anomalous dispersion regime at over 750nm as shown in Fig 3. This fibre has been used in previous experiments to successfully produce a SSFS peak at ≈1050nm.
A 12cm length of this fibre is packaged in aluminium with sealed cleanable ends in a device called a FemtoWHITE 800. This enables the PCF to be moved and adjusted without much risk of damage.
The FemtoWHITE core has a core diameter of 1.8±0.3µm and a Numerical Aperture (NA) of 0.38.

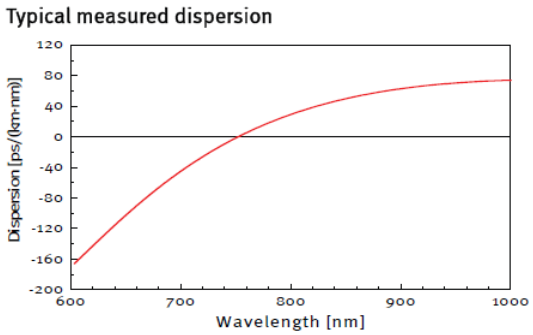

Fig 3. Dispersion curve for the NL-PM-750 fibre.

Equipment Set-up

The laser was focused into the fibre using a microscope objective. The x20 objective offers the best comprise between spot size and NA, suitable for the FemtoWHITE.

Firstly the fibre was aligned using a HeNe laser, to test the alignment, and check the fibre was not damaged. The focusing microscope objective was mounted on a XYZ stage to accurately couple into the fibre. At the output of the fibre a x40 microscope objective was used to collimate the beam. The laser was aligned roughly using two irises first, and then aligned parallel to the axis of the FemtoWHITE. The output spectrum was maximised by adjusting various mirrors and the XYZ stage. The complete set up is shown in fig 4.

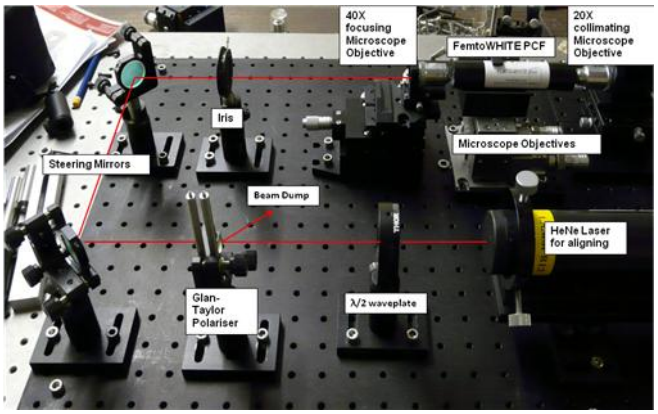

Fig 4. Equipment setup for preliminary aligning with HeNe laser.

Two different Laser pulses were used to understand the influence of laser pulse parameter on the fibre output. These were a tuneable Ti:S laser (MIRA, COHERENT) and a fixed wavelength ultrashort oscillator (Rainbow, Femtolasers). The set up and results for each were very different.

Mira

The Mira laser has a pulse length of approximately 100fs. The wavelength of the laser can be tuned from 830-900nm by adjusting the laser cavity. The average power of the input pulse generated by Mira decreases with longer wavelengths, as shown in Fig 5. At 850nm the average power is approximately 100mW more than at 900nm. This in turn means the peak power will be up to 30% less at 900nm than 850nm. The peak power at 850nm is approximately 10kW.

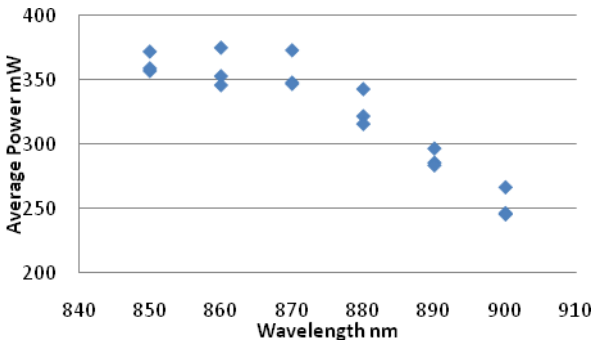

Fig 5. Mira maximum average power with wavelength.

The intensity was adjusted using a rotatable half-wave plate, with faraday isolator to prevent back reflections from disrupting the mode-locking. Varying the angle of the half wave plate causes the power to vary sinusoidally, as in Fig 6, but never quite reaches zero.

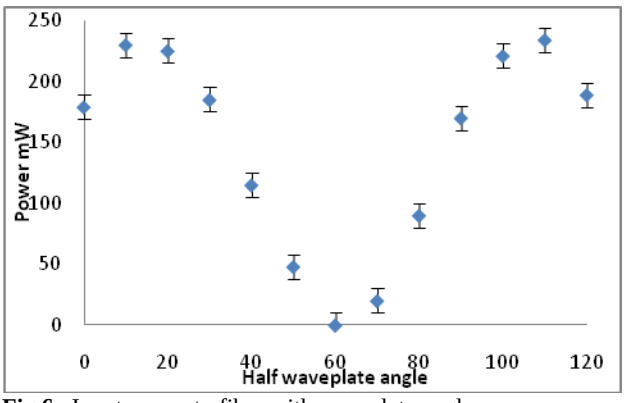

Fig 6. Input power to fibre with waveplate angle.

The laser was aligned and focused into the fibre using the above techniques.
At high powers bright greenish-white light was observed from the output of the fibre. When disperesed a prism, the green part of the spectrum was strongest, with hardly any blue noticeable as in Fig 7
.

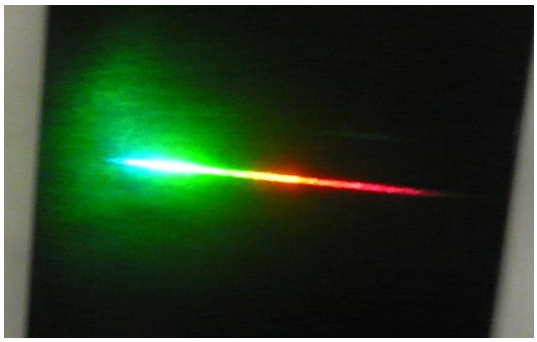

Fig 7. Visible light spectrum from the PCF when refracted with a prism.

The spectra were recorded using a custom made Labview program which plots an intensity graph. The intensity plot is useful to demonstrate how certain peaks in the output form when input variables are changed. The output spectrum was recorded while varying the power or wavelength.

Results

By turning the half-wave plate to gradually increase the input power the PCF output spectrum broadens. Initial broadening stages look similar to SPM broadening, with splitting of the main peak into 2, then 4 peaks as in Fig 8. With further increasing power, visible wavelength light is produced, and also a peak around 1000nm.

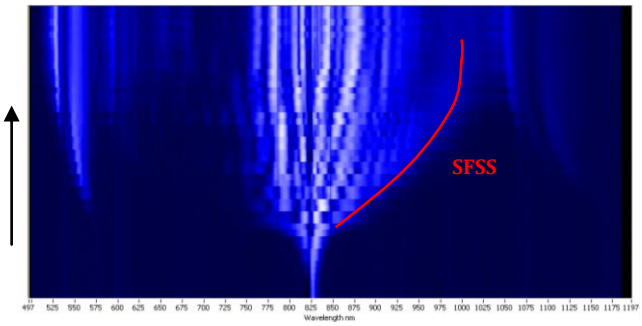

Fig 8. 830nm output spectrum with waveplate angle. Background removed, and intensity logarithmic scale for clarity.

In the long wavelength part of the spectrum there seems to be a broad pulse which moves to longer wavelengths with increasing power. This may be a SFSS as the red-shift increases with power and the pulse spectrum is approximately sech shaped as shown in fig 9.

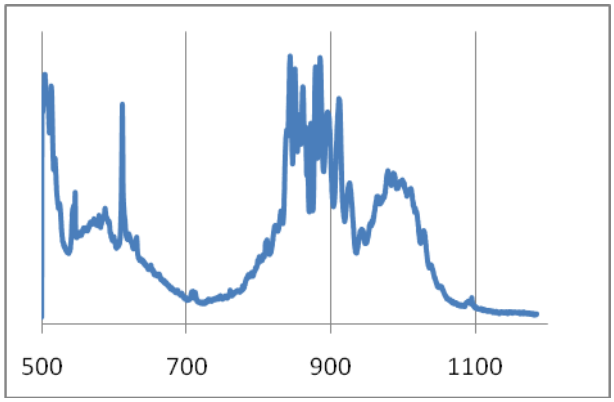

Fig 9 Output spectra for 870nm, 350mW input power.

At maximum power the various peaks start to combine and the beginnings of a supercontinuum form. With further propagation, dispersion and broadening effects blend out individual peaks to produce a smoother continuum.
At maximum power the pulse wavelength was varied from 830-900nm, the spectrums are shown in Fig 10. At 900nm the spectrum was seen to break down and become more chaotic, the soliton shift is less at longer wavelengths. This may be due to a slightly lower input power at long wavelengths.

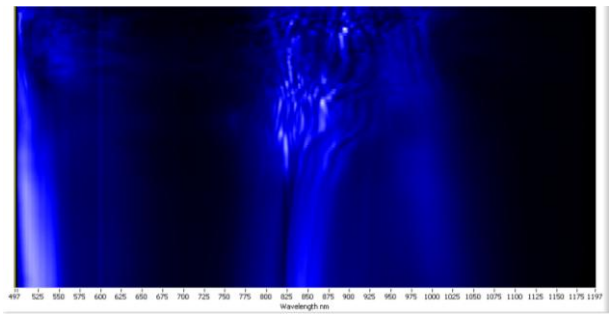

Fig 10. Spectra with changing input 830-900nm, background removed.

At full input power the Mira laser can produce reasonable power up to 1000nm.

Discussion

Using the Mira laser produced a spectrum of consisting of a broad 250nm bandwidth spectrum in the infra-red region, and also a separated peak in the visible. SPM is visible, and a possible SSFS has been produced. The fibre does not produce significant power at 1053nm, but by increasing power or fibre length it should be possible to produce a soliton peak at 1053nm.

Rainbow

The wavelength of Rainbow could not be varied. Due to the broad bandwidth it would have been unsuitable to use the same faraday isolator and half-waveplate combination as the Mira. So to vary the intensity a variable natural density filter was used. This means the input power on the below spectrums varies linearly. The peak power of the Rainbow is 40KW.

Results

The output spectrum of the rainbow does not broaden with increasing power in the same way as the Mira. Parts of the output spectrum seem to slowly appear with increasing power, instead of expanding from a central point as shown in Fig 11. At maximum average power 143mW the spectrum contains

many peaks, and has a bandwidth of ≈ 350nm, and is partly in the normal regime of the fibre. Individual features are difficult to identify in the final spectrum, although at the edges of the spectrum ripple like waves seemed to have formed.

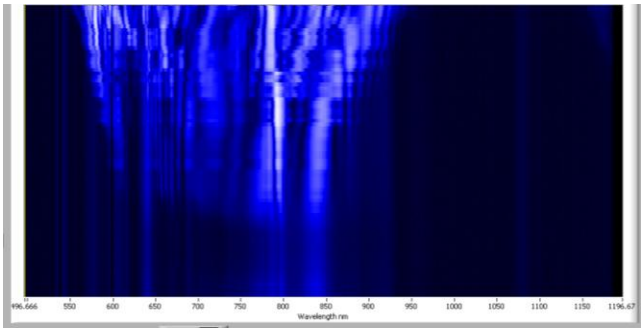

Fig 11. Output spectra with increasing power.

Because of the complexity of the spectrum it is difficult to tell which parts may be SSFS. The input pulse seems to shift towards longer wavelengths with increasing power. This is indicative of a self frequency shifting soliton. At high pulse the soliton seems to become split, possible due to trapping and interaction with parts of the pulse delayed by other processes.

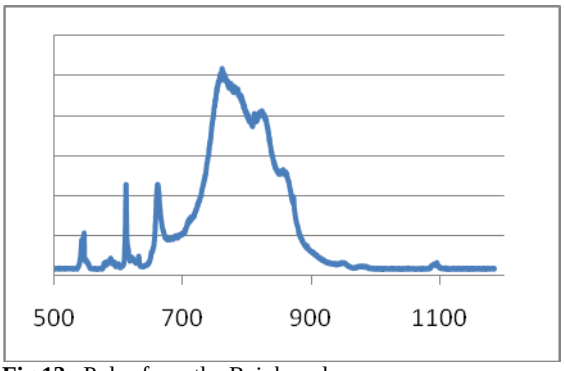

Fig 12. Pulse from the Rainbow laser.

As seen in Fig 12 the input pulse from Rainbow is very irregular. These irregularities may become amplified and produce different effects in the fibre from a Gaussian or sech shaped pulse of the same bandwidth.

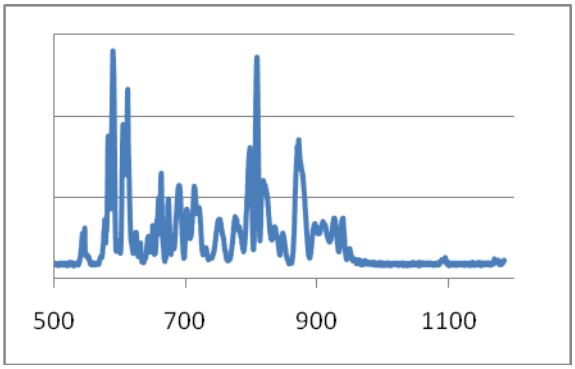

Fig 13. Maximum output spectra from the PCF.

The output spectrum only reaches 950nm at peak power, although it has broadened further into the low wavelength region than the Mira. The output spectrum at maximum power is shown in Fig 13.
The pulse may have undergone some chromatic dispersion whilst being focused into the fibre, due to its large bandwidth. This will have lowered the peak power and reduced some broadening effects.

Discussion

The Rainbow laser produces a spectrum of 350nm, stretching from visible into infrared. Individual phenomena occurring in the fibre are difficult to identify in the output spectrum. There is a possible SSFS on the long wavelength side of the spectrum, but it seems to have been trapped and split by other spectral components.
The output spectrum is less broad than one would expect for such a short pulse length. This may be due to chromatic dispersion in the coupling microscope objective, which would lead to temporal dispersion in the pulse.
The average power for the Rainbow is less than for the Mira, but due to the short pulse length the peak power is higher.
The pulse spectrum is also very irregular. These irregularities may be exaggerated and increased during propagation, and will produce a more unexpected spectrum. Using a smooth sech or Gaussian shaped pulse should minimise any unusual effects.
The maximum wavelength produced is at 950nm, this is very far from the desired 1043nm. Using a longer fibre, or increasing the input power should produce longer wavelengths, although overall the Rainbow laser has proved to be less effective than the Mira.

Conclusion

Using a 100fs pulse with 350mW average power produced more energy in the 1000nm region than a 60fs pulse with 143mW average power. The difference is likely to be due to lower power in the 60fs, and chromatic dispersion in the microscope objective. A self frequency shifted soliton was seen with the Mira laser at 1000nm. Using a longer fibre or providing more input power with either laser should shift the soliton to longer wavelengths, to produce enough energy at 1053nm to seed Vulcan.

References

1. "Photonic Crystal Fibres" Russell, Science **299** 358 (2003)
2. "Supercontinuum Generation in Photonic Crystal Fibre" Dudley, Reviews of Modern Physics **78** (2006)
3. "Widely Tuneable Femtosecond Soliton Pulse Generation at a 10GHz Repetition Rate by Use of Soliton Self Frequency Shift in Photonic Crystal Fibre" Abedin, Optics Letters **28** 19 (2003)
4. "0.78-0.90µm Wavelength Tunable Fermtosecond Soliton Pulse Generation using Photonic Crystal Fibre" Nishizawa, IEEE Photonics Technology Letters **14** 7 (2002)
5. "Photonic Crystal Fibres – A New Class of Optical Waveguides" Broeng, Optical Fibre Technology **5** 3 (1999)
6. http://www.femto-st.fr/en/Popularization/An-introduction-to-phononic-crystals.php (27/5/11)
7. Nonlinear Fibre Optics – Govind P. Agrawal

Study of the 10PW Front-end Contrast

Contact *Andrey.lyachev@stfc.ac.uk*

Andrey Lyachev, Ian Musgrave, Marco Gallimberti, Cristina Hernandez-Gomez, Ian Ross and Yunxin Tang

Central Laser Facility, STFC, Rutherford Appleton Laboratory, HSIC, Oxfordshire, OX 11 0QX, UK

Introduction

In our last contribution [1] we reported on the initial performance of a front-end for the Vulcan 10PW upgrade. In this contribution we report on the contrast studies conducted using this system. A schematic overview of the design of the front-end system is shown in figure 1. The initial task is to generate a pulse with sufficient bandwidth to support a 30fs pulse these pulses are then amplified to 100s of µJs on the picosecond timescale. This limits the temporal window of the parasitic fluorescence that seeds the rest of the system to the duration of the pump pulse ~ 10 ps. This clean pulse is then stretched to 1.87ns before further amplification to the joule level. In this paper we will discuss the different components in turn and their influence on the output of the system.

Fig. 1. Schematic of the front-end.

Seed generation and mJ OPA stages pumping

The initial seed is generated using picosecond timescale OPCPA to limit the duration of the initial parametric fluorescence that seeds the rest of the system. To generate the broad bandwidth required the technique of chirp compensation is employed [2] this scheme is operated in a collinear non-degenerate geometry which is instantaneously narrowband. However, for the same phase matching angle there are a number of combinations of signal, pump and idler wavelengths that satisfy the phase matching criteria. This process was described in detail in our recent publication [3] and forms the first stage of the system which combined with an additional 2 stages increase the seed energy to 500µJ. The scheme requires the relative chirps between the signal and pump to be well controlled. In our case we have a phase matching angle of 31^0, a signal chirp of 17.5 nm/ps and a pump chirp of 1 nm/ps. This enables us to generate pulses that have a bandwidth of 140 nm.

A schematic of the three stage system is shown in figure 2, the seed and pump pulses are formed by spectrally dividing the output of a Ti:Sapphire laser using a spectral beam splitter. A portion of the spectrum with 150 nm bandwidth centered at 720 nm is used as the seed whilst a 20 nm section of the spectrum at 800 nm is used to form the pump beam. The pump beam is stretched in a grating stretcher to ~ 10 ps before being amplified to 1.8mJ in a multipass amplifier (Femtolasers Compact Pro). The amplified pump pulse is then frequency doubled to 400 nm in BBO1. The seed pulse is stretched in a prism stretcher to ~ 10 ps. The pump and seed beams are then mixed in crystal LBO1 amplifying the seed and generating an idler signal centered at 910 nm and having ~ 140 nm FWHM spectrum as shown in Fig. 3. There is a small non collinear angle between the pump and signal beams to enable the separation of the signal and idler beams. The pump fluence for this stage is 150mJcm^{-2} and the incident seed energy is 0.5nJ. The energy contained in the idler after this first stage is ~2 µJ this idler beam then forms the seed beam for the subsequent stages.

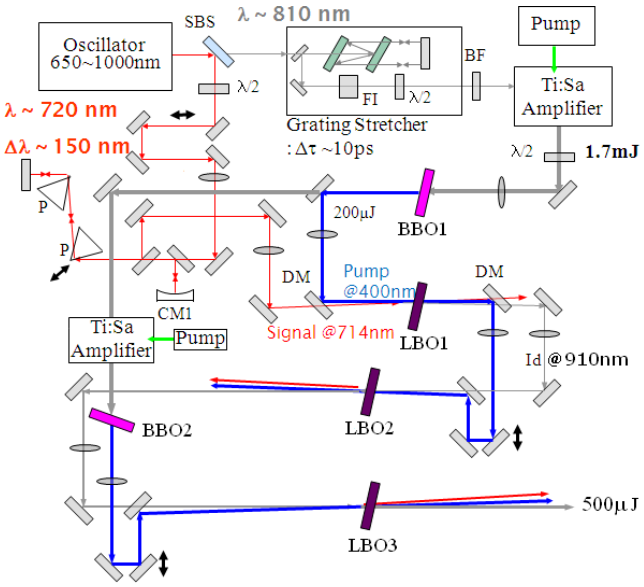

Fig. 2. Broadband pulse generation and mJ level OPA stages layout.

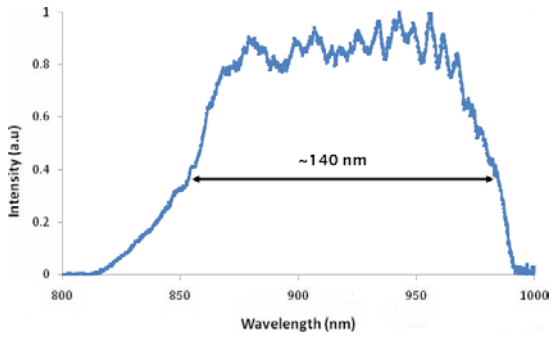

Fig. 3. Spectrum of the idler generated at the first stage of mJ level OPA.

The undepleted pump from the first stage is relayed to LBO2 to act as the pump for the 2nd stage. The 910nm idler from the 1st stage is relayed to form the seed of the 2nd stage with the 720nm beam from the 1st stage blocked in the near field between the 2 stages. The pump fluence in the second stage is 170mJcm^{-2} and the output pulses have 25 µJ retaining the bandwidth.

To further increase the energy a 3rd stage is used. The pump beam is formed by amplifying the unconverted 800nm from BBO1 in an additional Ti:Sapphire amplifier. This additional Ti:S amplifier increases the pump pulse energy for stage 3 to ~ 30 mJ at 800 nm . This compact additional Ti:Sa amplifier is a 3-pass bow-tie geometry pumped from both ends. The amplified signal is then frequency doubled to the required 6.5 mJ at 400 nm pulse for pumping the third OPA stage and delivering 500 µJ amplified output pulse retaining the bandwidth.

To demonstrate that the output of this system can be compressed a simple single pass compressor was established for the 910nm output. This comprised of a single block of 40.5mm SF10 and a grating compressor with 1200l/mm with a separation of 9.5mm and an incidence angle of 12^0. A single shot SPIDER was used to measure the pulse to be 25fs. The contrast of the seed was then measured using a SEQUOIA. The contrast trace is shown in figure 4. As can be seen the dynamic range achieved with this combination of energy and pulse duration was 5 orders of magnitude. The contrast of the pulse is 10^5 at -1.2ps the shoulder that the pulse sits in that goes from -1ps to 0.5ps is attributed to incomplete compression because the shape of this region could be influenced by the separation of the grating compressor.

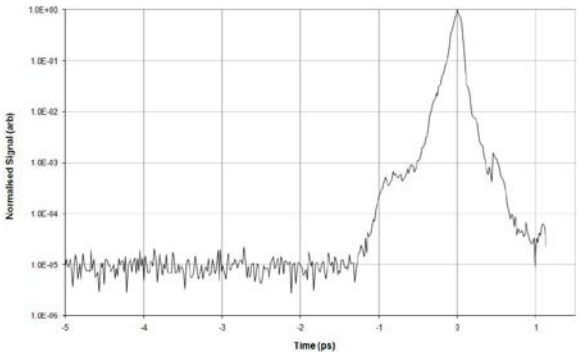

Figure 4 Contrast of the compressed output from the seed generation scheme.

Seed pulse stretching

To evaluate the performance of an all OPCPA front-end system amplifying a broad band seed pulse to the Joule level a test CPA scheme was designed to increase the pulse length to several nanoseconds. The pulse stretching is obtained by using a double pass stretcher [7] which has been modified to increase its bandwidth to 140nm and is limited by the size of the available gratings. A schematic of the stretcher and the seed pulse injection is presented in Fig. 5.

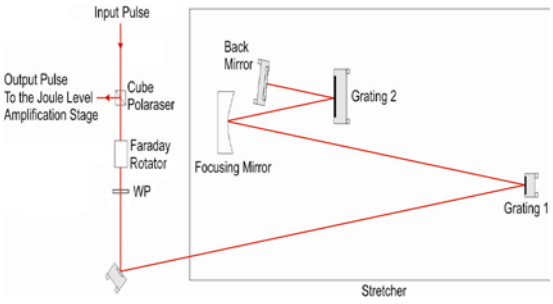

Fig. 5. Schematic of the stretcher injection.

The pulse is incident at an angle on grating 1 which has a grove density of 1480 lines per mm and is tilted to be at the Littrow angle for 900nm. The pulse is then directed to a focusing mirror f = 500 mm where the beam is off axis. The centre of the radius of curvature of this mirror is such that it is vertically at the centre of the gratings but placed horizontally between them. After the mirror the pulse is incident on gating 2 before being retro-reflected by the plane mirror which is placed close to the image plane of the mirror. To minimize the chromatic aberrations introduced by the stretcher it requires a beam waist between the first grating and the curved mirror. The control of the pulse injection to the stretcher and the output pulse rejection is achieved using a polarizing beamsplitter cube and the combination of a Faraday rotator and a a half wave plate. The stretcher demonstrates ~ 50 % transmission efficiency delivering ~ 1.87 ns output pulses. There is a spectral loss of the output pulse spectrum due to size of the second grating in the stretcher introducing a hard clips at 830 and 970nm.

Joule level OPA stages

After stretching the pulse is imaged and expanded into the first crystal of the Joule level OPA amplification scheme. The amplification for this section is achieved in two stages as schematically presented in Fig. 6.

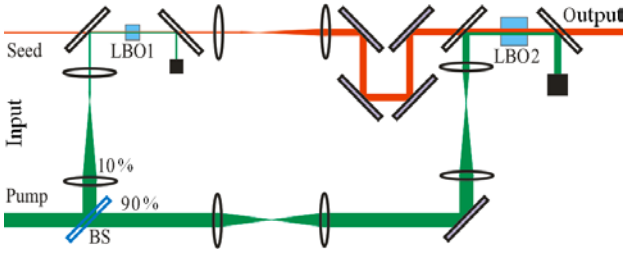

Fig. 6. Joule level OPA stages layout.

The setup involves usage of 19 mm and 20 mm long LBO crystals respectively for each stage. The crystals have been placed into electrically heated metal ovens mounted on 4-axis stages. The OPA process is a non-collinear type-1, where the seed and idler have the same polarization (set as P) and the pump is orthogonal to this (set as S).

The seed beam line from the LBO1 to LBO2 has been established by magnifying the beam diameter from 2 to 10 mm and image relaying it using a vacuum telescope. An optical delay line is introduced in the seed path providing the timing adjustment between the interacting pulses on LBO2.

The pump beam line has been built up with three vacuum telescopes to provide collimated and image relayed beams of about 4 mm in diameter on the LBO1 and 10 mm on LBO2. The pump laser delivers 4.5 J pulses at 532 nm at a 2 Hz repetition rate with a square temporal profile and spatial top hat profile (Continuum custom laser). A combination of 90/10 beam splitter, half wave plates, polarisers and beam dumps has been arranged to provide pump energy control for both stages of amplification and deliver up to ~ 3 J/cm^2 pump fluence on each crystal. The undepleted pump beams are blocked after each crystal.

At 3J/cm^2 the maximum small signal gain (SSG) on stage 1 of the Joule level OPA was detected at ~ 400 giving over 12 mJ output seed energy at this stage for 20μJ of input seed energy. This pulse was further amplified on stage 2 of the J level OPA meeting close to expected SSG value of ~ 40 and having over 0.4 J of output energy at a pump fluence of 2.5J/cm^2. Evolution of the amplified pulse spectrum on the Joule level OPA stages is shown in Fig. 7. As mentioned previously the initial seed spectrum (blue trace) is limited by the size of the gratings in the stretcher. Further loss in spectrum of the amplified pulse is caused by the bandwidth of the broadband mirrors, although providing ~ 100 nm bandwidth of the output pulse spectrum.

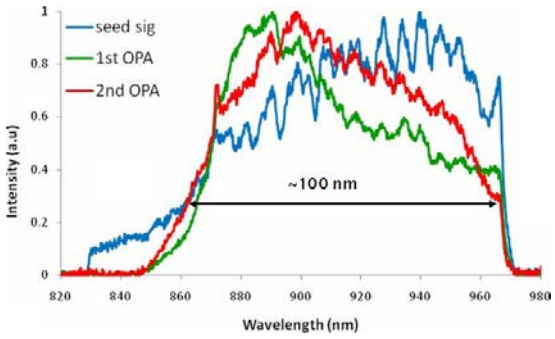

Fig. 7. Joule level OPCPA output pulse spectra.

Pulse compression

To test how compressible the amplified pulse is, the output beam from the Joule level OPA stages was injected into a 4 grating double pass compressor. A schematic of the compressor is demonstrated in Fig. 8 viewed from the top. This geometry was imposed on the compressor due to the size of the available gratings.

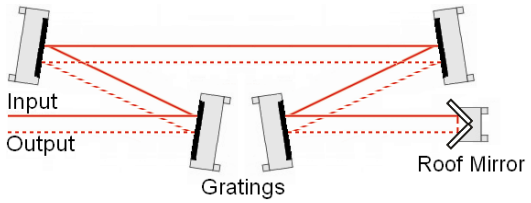

Fig. 8. Schematic of the compressor, top view.

The four gold gratings have a line density of 1480 l/mm and are used at Littrow in an out of plane design. It is double passed using a roof mirror to displace the beams on the return path. We were able to compress our pulse to 35 fs using a SPIDER to measure the pulse after compression as shown in Fig. 9.

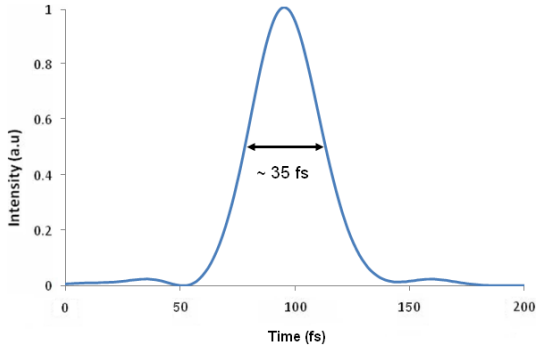

Fig. 9. Pulse duration of the final compressed pulse measured by Spider.

The contrast of the compressed output has been measured using a combination of photo-diodes and a SEQUOUIA. The diode system had a dynamic range of 10 orders of magnitude and showed that there was no parametric fluorescence within this range on the nanosecond time scale. The contrast trace measured using the SEQUOIA is shown in figure 10. As can be seen there are a number of features, the pulse sits on a shoulder that starts at 30ps before the main pulse. This is due to fluorescence from the 3rd stage of the seed generation scheme; further work is required to determine why it starts at 30ps. This could be due to scattering in the stretcher reported elsewhere [5].

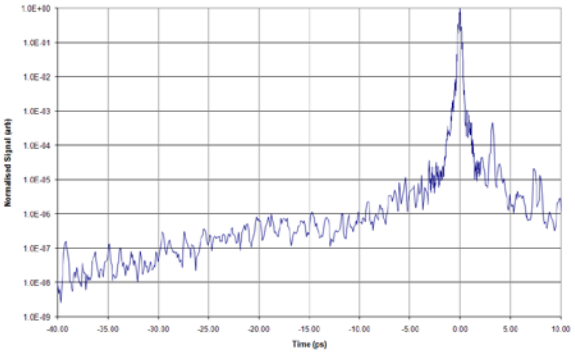

Figure 10. Contrast measurement of the close in contrast.

Conclusion

In conclusion we have constructed and evaluated an all OPCPA front-end scheme for seeding large aperture high peak power OPCPA systems. We have demonstrated the generation of a seed source at 910nm with sufficient bandwidth to support 35fs pulses. These seed pulses have been amplified on the picosecond timescale to the sub millijoule level and compressed to 25fs, limited by the compressor. The measurement of this contrast shows that the pulses are clean enough to seed large aperture systems.

References

1. A. Lyacheve et. al. '10PW front-end characterization' CLF Annual Report 08-09, p271-272 (2009)
2. K. Osvay, I. N. Ross, "Broadband sum-frequency generation by chirp-assisted group-velocity matching," J. Opt. Soc. Am. B **13,** 1431 (1996).
3. Y. Tang, I. N. Ross, C. Hernandez-Gomez, G. H. C. New, I. Musgrave, O. V. Chekhlov, P. Matousek, J. L. Collier, "Optical parametric chirped-pulse amplification source suitable for seeding high-energy systems," Opt. Lett. **33(20)**, 2386 (2008).
4. I. N. Ross, A. J. Langley, P Taday, "A Simple Achromatic Pulse Stretcher", CLF Annual Report, 201 (1999/2000).
5. Hooker C, Tang Y, Chekhlov O, Collier J, Divall E, Ertel K, Hawkes S, Parry B, Rajeev P.P "Improving the coherent contrast of petawatt laser pulses" Optics Express **19** 2193-2203 (2011)

Two beam spatial phasing with a CW laser

Contact *jonathan.phillips@stfc.ac.uk*

P. Jonathan Phillips, C. Hernandez-Gomez, I. Musgrave, J. Collier

Science and Technology Facilities Council, Rutherford Appleton Laboratory,Harwell Science and Innovation Campus, Didcot, OX11 OQX

Introduction

High average powered lasers are attractive owing to their potential for a diverse range of experiments. The power extractable from current laser systems is limited by the size of the amplifying medium, damage thresholds and other optical components. Other important additional factors limiting the scale of amplifiers for repetitive systems are ASE, laser material growth, heat effects and depolarization. Another way of achieving these high power requirements is to combine several beams into a monolithic beam, which immediately reduces the requirements for the amplifier to a more modest level.

We have developed a system to investigate a method for spatial recombining; the wave front methodologies was previously reported in CLF annual report 2010[1]. We have a Ti:Sapphire laser which can produce pulses of 100 fs , ~5 nJ of energy per pulse and has a wavelength tuning range of 950-1080 nm. In these experiments we are using the laser in a CW mode. As shown in Figure 1, the optical layout expands the beam up to 120 mm beam diameter from the laser. It is currently subdivided into two beams by using two mirrors, each 50 mm square. Each mirror has independent control of the tip /tilt. Mirror 2 is on a translation stage for control of the piston. There is an actuator for each of the axis, with a resolution of 30.5 nm and a backlash of ~ 6 μm. Each actuator is connected to a computer via a control box. The beam from the two mirrors is imaged relayed to a Wave Front Sensor (WFS) for wavefront analysis. There is a beamsplitter in the path before the WFS so that the beam can go to an 8-bit CCD camera for an image of the far field. The far field image is useful for two reasons. The first being, it can act as a starting reference for the position for primary sub aperture. Secondly it is used to bring the two far field focuses closely together so that the WFS can then overlap them. The WFS camera and the 8-bit CCD camera are attached to a computer for data retrieval. The WFS is a PHASICS SID 4[2] camera which uses the quadriwave lateral shearing interferometer (QWLSI) method[2]. This creates an interference pattern between the two wavefronts from the sub apertures and the phase information and piston measurement can be extracted from this pattern, this can be seen in Figure 2. The individual tip and tilt of each mirror is calculated from two further sub aperture either side of the interference of the two beams. These measurements are self referenced, simplifying implementation. It has been shown that the piston measurement accuracy with this system can be estimated to be 40 nm or less.

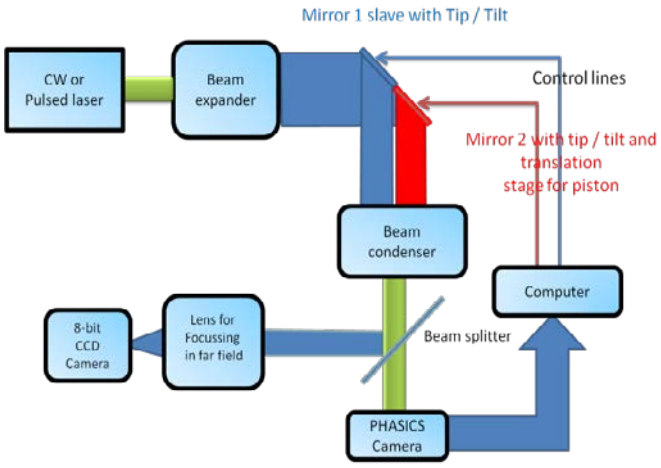

Figure 1: Schematic diagram of the laboratory setup.

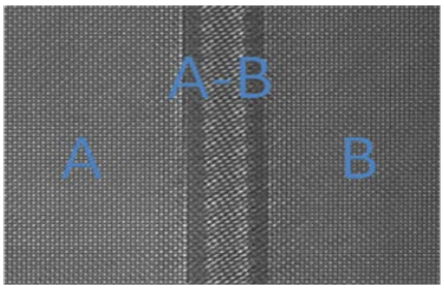

Figure 2: Shows a camera image depicting the three sub apertures. Sub aperture A (primary) and B (secondary) coming from the individual mirrors, with the A-B sub aperture from the interference from the two mirrors.

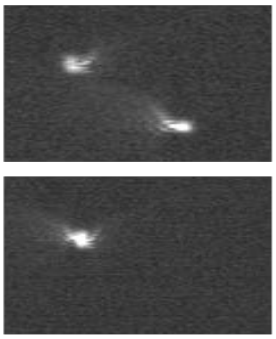

Figure 3: Shows the two spots on the far field camera (top image) when separated and then when bought together (bottom image) in a coherent manner.

The close loop program is written in LabView by the following methodology:-

1. That the if the two far field foci (Figure 1c upper image shows the two far fields in this state) are not overlapped then the primary sub aperture beam has both the tip and tilt minimised to within +/- 0.15 μrads by the PHASICS camera.
2. Then the 8-bit CCD camera is used to see how far away the two far field beams are. Tip and tilt of the second aperture is manipulated until the two beams are within 60 μm of each other in both the x and y planes.
3. PHASICS camera takes over to reduce the tip and tilt to within +/- 0.15 μrads of the secondary sub aperture beam.
4. The next step is to check that the piston measurement is less than +/- 0.15 of a wavelength. This is achieved by the movement of the translation stage of the secondary sub aperture.
5. Control software then checks that the far field images are overlapped (Figure 1c shows the two far field images overlapped).
6. A loop is then instigated to go back to 1.

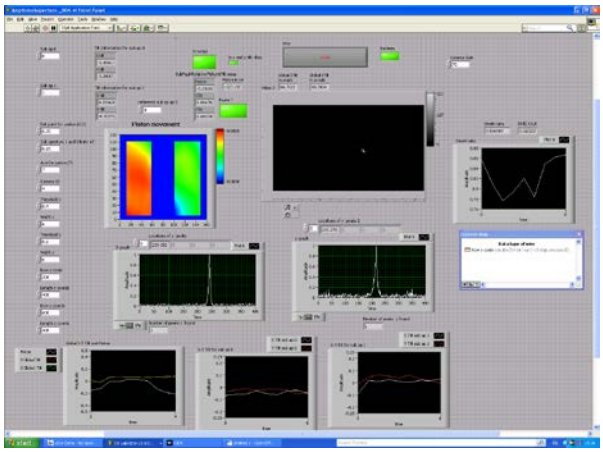

Figure 4: Shows the software for monitoring the coherent overlap of the two pulses.

Figure 4 shows the software as described in the steps above. This software displays the tip and tilt measurements of each sub aperture as well as the piston error. As each measurement is taken then they are displayed onto a graph so that the user can see when the parameters fall out of the set points. A graph of the Strehl ratio is also displayed. System is currently slow to operate as there is backlash in the actuators. In future this part can be increased in speed by including a spatial read back function in the actuator.

We are able to measure the Strehl ratio with the use of the formulae shown in Equation 1.

$$S = e^{-\left(\frac{2\pi\sigma}{\lambda}\right)^2} \qquad (1)$$

λ = Wavelength of wavefront being measured (nm).The wavelength is 1030 nm.

σ = RMS value of wavefront aberrations. (A measured value typically is 0.06022 λ)

Using Equation 1 and global RMS measurement of the wavefront we are able to predict a Strehl ratio of 0.82.

Future developments

This project is funded by the LASERLAB-EUROPE II fund.

In the future temporal lock of the pulses will be explored.

In is also envisaged that this system we be implemented on to the Astra-Gemini laser system[4], which has two beams at 800 nm with each pulse at 30 fs.

We are also going to include four beams in the test bed setup with the same aperture size and then spatial phase these together.

Conclusions

We have achieved the spatial phasing of two CW beams with the use of a PHASICS camera and a normal CCD and written software so that the system can be used in closed loop.

References

1. "Experimental setup in the Vulcan HaPPIE laboratory for Multi-beam combination to achieve Diffraction limit pulses", STFC,CLF Annual report, 2009-2010
2. PHASICS ,A, XTEC Bat 404, Campus de L'Ecole Polytechnique, Route de Saclay 91128, Palaiseau, France
3. S.Mousset, C. Rouyer, G.Marre, N. Blanchot, S. Montant, B. Wattellier, "Piston measurement by quadriwave lateral shearing interferometry" Optics Letters, 31,17, 2634-2636 (2006)
4. C.J. Hooker, J.L. Collier et al.,"The Astra Gemini project-A dual-beam petawatt Ti:Sapphire laser system" J.Phys. IV France 133 (2006) 673-677

Improvements in the Vulcan Picosecond OPCPA – 50% conversion of pump to signal and compression back to 100fs. The potential of using OPG's (or continuum generation) for seeds of off harmonic probes

Contact *waseem.shaikh@stfc.ac.uk*

Waseem Shaikh, Ian Musgrave
Central Laser Facility

Introduction

We have previously reported (1) on the generation of a broad bandwidth picosecond OPCPA system which is now routinely used as the seed for the nanosecond Vulcan OPCPA - by providing ~110µJ picosecond pulses as the seed for the second and third stages of the Vulcan OPCPA preamplifier, the nanosecond contrast in Target Area Petawatt has been improved by at least two orders of magnitude (2).

Picosecond OPCPA – 50% pump to signal conversion.

The picosecond OPCPA routinely delivers ~110µJ of energy using a compact CPA system pumped by 550µJ of pump light. The 100fs pulses from the Ti-sapphire laser are stretched to 3ps in a compact single grating stretcher before being amplified by the 10ps pump pulses provided by the picosecond regenerative amplifier. This reduced level of stretch is required to ensure efficient amplification across the full bandwidth of the seed (3). 110µJ represents ~20% conversion efficiency from pump to signal. The signal pulse seeding the OPA is only 3pJ, equivalent to 10^7 photons.

To further increase the energy extraction of the pump pulses, a second OPA was set up - pumped by the residual pump from the first stage. For the second stage OPA, another 15mm long BBO is used. The signal is expanded using telescopes by a factor of 3.3 and the pump by 1.5 so that both pump and seed beam sizes are matched. This arrangement is shown in Figure 1.

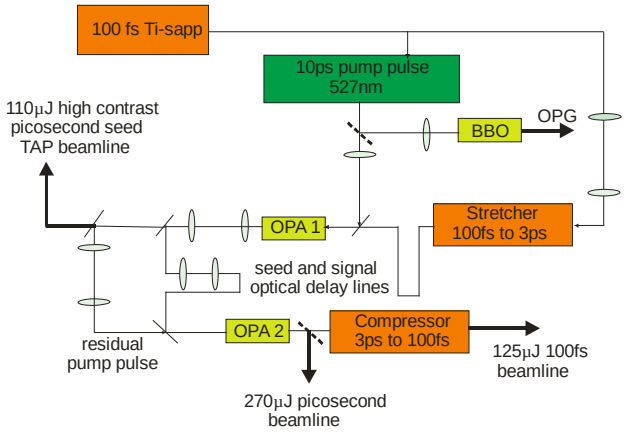

Figure 1. Schematic of two stage OPCPA system. The 'dashed' lines represent removable mirrors.

We have obtained a stable signal output energy in excess of 270J, representing close to 50% of the 550µJ of pump energy available from the picosecond pump laser. This could be used to increase the picosecond input into the conventional TAP OPCPA pre-amplifier (or to potentially act as a seed for a TAW OPCPA arrangement, eliminating the need for the pre-amplifier 9's.**)**. The spectral output of the seed (black trace) and fully amplified OPCPA (red trace) are shown in Figure 2.

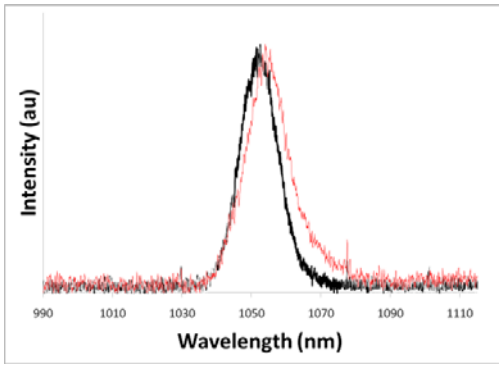

Figure 2 Spectral Output of Dual Picosecond OPCPA

Signal/idler compression

The ability to compress this level of signal energy would represent a very useful addition to the front end capability. To compress the amplified OPCPA output, a second compressor, identical to that used to stretch the femtosecond seed pulse was constructed. Because the signal and idler pulses are oppositely chirped, a simple translation of the mirror and lens, located

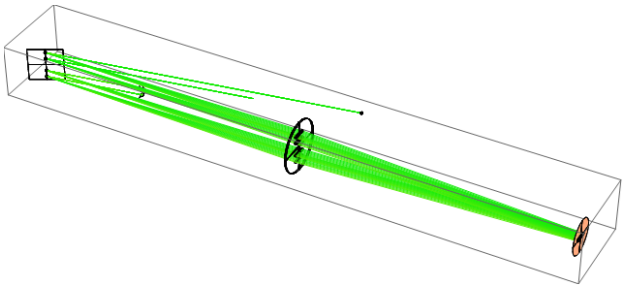

Figure 3. Stretcher and/or Compressor

on a separate translation stage, allows both signal or idler pulses to be compressed. Figure 4 shows the compressed output from the picosecond OPCPA, taken using the seed source.

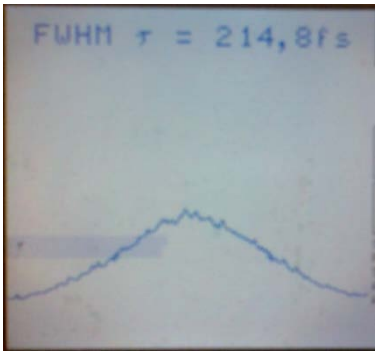

Figure 4. Compressed 'signal'

This energetic femtosecond seed source could be used for the development and testing of continuum sources. Measurements of contrast (using third order Sequoia techniques) could help determine the picosecond contrast in TAP.

OPG seed generation at off resonance wavelengths.

The intensity provided by this compressed picosecond system has enabled preliminary experiments to be conducted on potential sources of well synchronized off harmonic seeds. These could be used to seed other lasers which require different seed wavelengths. (These have been produced using Ti-sapphire femtosecond sources and photonic crystal fibers (4)). The spectral output shown in Figure 5 was obtained in an OPG arrangement (Figure 1) where the residual picosecond pump was weakly focused into a 10mm long BBO crystal. OPG sources tend to favour long wavelength generation whereas continuum sources shorter wavelengths. As in the picosecond OPA system, we only require ~10^7 photons to seed an OPA system pumped by a more energetic pump source to provide millijoule level probes.

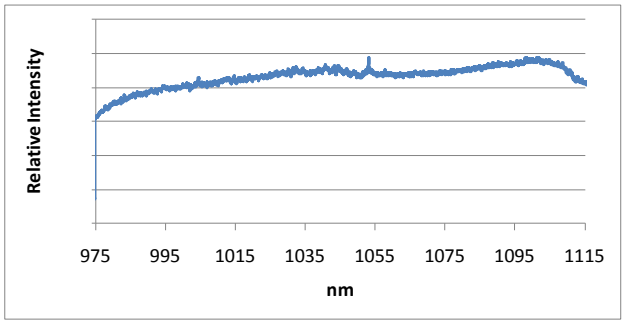

Figure 5. Broadband spectral output of an OPG pumped by the residual picosecond green**.**

The ability to generate these broadband sources, and the use of Spatial Light Modulator (SLM) (5) to spectrally shape the spectral source at the spectral plane of a stretcher before amplification should allow the generation of arbitrary shaped transform limited pulses of arbitrary wavelength. This could be achieved using all reflective CPA system with a single grating, (as shown in Figure 6) incorporating the spatial light modulator at the mirror.

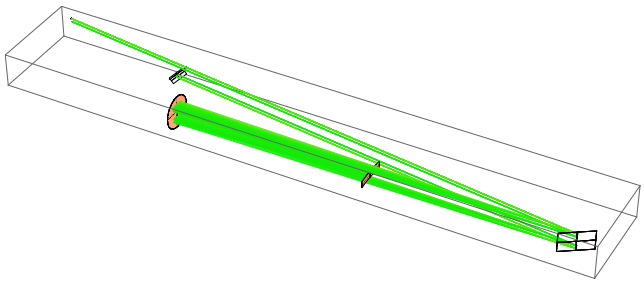

Figure 6. Achromatic CPA system incorporating a potential SLM at the spectral plane.

References

1. W.Shaikh et. al. CLF Annual report 2008-2009 pp 292-293
2. I. Mugrave et. al. Appled Optics Vol **49** Issue 33 pp 6558-6562
3. J.A.Fulop et. al. Shaping of Picosceond pulses for pumping of optical parametric amplification. Applied Physics B Vol. **87** 79-84 2006
4. http://www.nktphotonics.com/fiber
5. http://www..bnonlinear.com

Vulcan 10PW Project : Design of the Long Pulse Pump Laser

Contact *Trevor.Winstone@stfc.ac.uk*

TB Winstone, S Blake, A Frackiewicz, M Galimberti, S Hancock, R Heathcote, C Hernandez-Gomez, P Holligan, A Kidd, IO Musgrave, D Pepler, W Shaikh

Central Laser Facility

STFC Rutherford Appleton Laboratory, Chilton, Didcot, Oxon. OX11 0QX

Introduction

The Vulcan 10PW facility [1] requires a Long Pulse Pump Laser to transfer energy to the seed pulse within the large aperture Optical Parametric Chirped Pulse Amplification (OPCPA) [2] stages. To pump the two stages of the OPCPA amplifier two similar beams are required.

Figure 1: schematic of anticipated laser layout

The systems being considered are outlined below.

The specification of each of these two beams is for 600 J at 527 nm in a temporally shaped flat topped 3 ns pulse. The seed pulse is generated by the use of a shaped long pulse (SLP) oscillator. The output of this SLP would then be amplified by well known methods based on existing technology used in the Vulcan laser, in the form of a rod amplifier chain and a disc amplifier chain. The current anticipated design would use a combination of existing 108 and 208 amplifiers in a multi-pass disc amplifier architecture with new amplifiers using a rectangular slab technology. These pulses will be frequency doubled to 527 nm before being used to pump the OPCPA crystals.

Shaped Long Pulse(SLP) Oscillator

To overcome the distortion of the pulse shape that inevitably occurs during saturated amplification to high energies in rod and disc amplifier chains, there is a requirement to provide a temporally shaped input pulse from a Shaped Long Pulse Oscillator (SLP) which can pre-compensate for these effects. The Vulcan Glass Laser System at the Central Laser Facility has developed a long pulse shaping system [3]. The 10 PW Facility will take advantage of this development and use a similar system as the seed for the pump pulse. The SLP oscillator will produce temporally shaped seed pulses from an intensity modulated fibre optic oscillator based on single mode fibre systems, driven by an Arbitrary Waveform Generator (AWG). This shaped pulse of ~100 pJ will then be amplified in a regenerative amplifier to the milliJoule level.

A continuous wave laser is used to generate a shaped pulse within a fibre optic intensity modulator, which is driven by an Arbitrary Waveform Generator (AWG). The output of these fibre modulator systems is limited to several nJ because of their power handling capabilities. A key aspect of this system is the diode pumped regenerative amplifier (Figure 2) to amplify to the mJ level.

A telescope is used to match the beam radius of the delivery fibre to the amplifier cavity. They pass through a Faraday isolator that is used to switch the output of the amplifier by rejecting the returning pulses. The cavity is formed by two concave mirrors separated by 1.5m enabling amplification of pulses up to 10ns in duration. The cavity has been folded to reduce its footprint and enable end pumping with two mirrors next to the Nd:YLF rod, both highly reflecting at 1053nm and anti-reflecting at 805nm, the pump wavelength. The pump power is provided by 2 fibre coupled 25W CW diodes operating at 805nm. The pumping is achieved by imaging the output of the pump delivery fibres to the centre of the crystal using a telescope comprising 35mm, 100mm and 200mm focal length lenses. This combination of focusing lenses has been selected to minimise the risk of thermal fracture of the Nd:YLF crystal.

The regenerative amplifier is operated at 10Hz and the pulses are amplified to the ~0.5mJ level. The output Pockels cell is used to remove unwanted prepulses produced within the regenerative amplifier. Temporal stability and beam quality of any seed source are both important issues for injection into a low repetition rate large glass laser like Vulcan. The shot to shot stability of the regenerative amplifier has been measured to be better than 5% over long periods of time – a key benefit of diode pumping.

The existing SLP has proved that we can meet the pulse shape requirements, but further tests are required to ensure energy stability and robustness of the system.

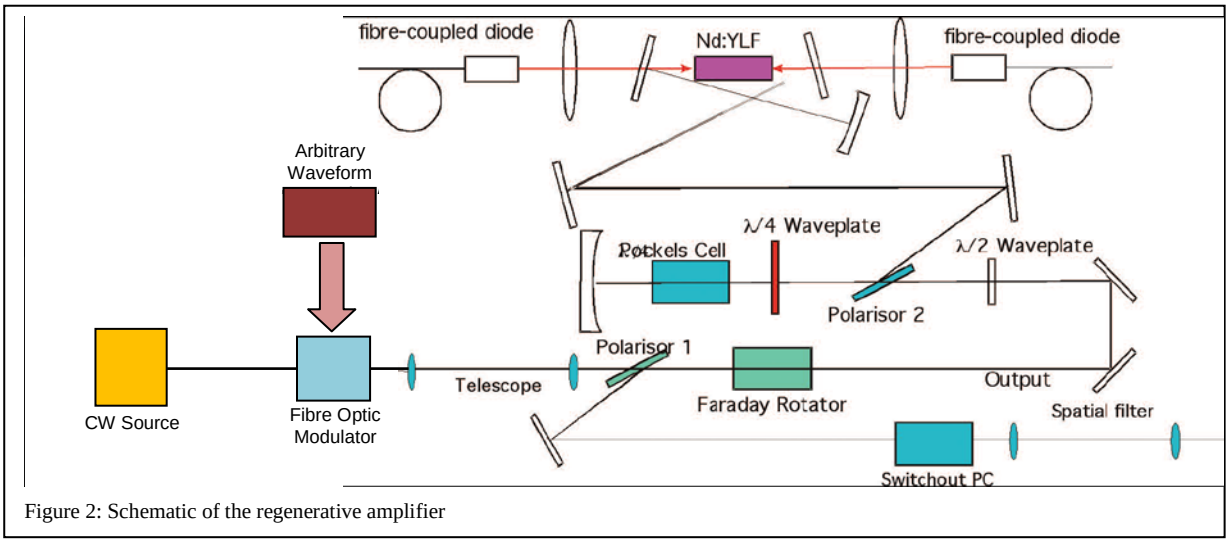

Figure 2: Schematic of the regenerative amplifier

Rod Amplifier Chain

A rod amplifier chain is required to amplify the beam from the mJ level at the output of the oscillator to the Joule level prior to injection into the final disc amplifier chain. The 10PW Facility will use Quantel [4] rod amplifier heads and power supplies, similar to those used in the Vulcan Laser System. This type of technology is well known and has proven to be reliable. Although the commercial amplifier heads that will be used are similar to those designed in-house there are some differences. In particular the doping level and length of the rods exposed to the flashlamp light differ. It will therefore be necessary to undertake gain tests to adequately determine the detailed design of the system and achieve the required level of amplification.

The amplifiers available to this project are Quantel manufactured heads and power supplies in the form of one 9 mm, one 16 mm, one 25 mm and one 45 mm. This is identical to the rod amplifier chains currently used in Vulcan.

The design is based upon the current Vulcan rod amplifier chain. This has operated successfully over the past 22 years and provides a good basis for the rod amplifier system of the 10PW Long Pulse Pump Laser.

After the Shaped Long Pulse oscillator a double passed 9 mm amplifier will be used to boost the energy to the tens of mJ level before being injected into an air spatial filter. The remaining amplifiers will be arranged in a single pass line from 16 mm amplifier through to the output 45 mm rod amplifier. The focused intensity after the 16 mm rod amplifier is sufficiently high to break down air so vacuum spatial filtering (VSF) is applied. These VSFs will clean the beam and also increase the beam size, hence lowering the beam fluence at the output relative to the input. After each amplifier stage will be an isolation component, in the form of either a Faraday rotator or a Pockels cell, each coupled with crossed polarisers to ensure rejection in the event of the isolation component failing to operate. A potential layout of the rod chain is shown in figure 3.

Amplifier	Energy at output	Fluence at output
Double passed 9	15 mJ	0.15 J/cm^2
16	203 mJ	0.22 J/cm^2
25	1.26 J	0.49 J/cm^2
45	5.5 J	0.55 J/cm^2

Table 1: Energy and fluences at different stages of the rod amplifier chain

At the end of the rod chain a delay line will be required on one of the beam lines to control the timing of the pulse arriving at the final OPCPA stage.

To ensure that the gain of the rod amplifier chain will meet the required level a series of tests will be conducted on each amplifier. A modulated pulse will be amplified through each rod amplifier in turn and the ratio of the amplified pulse energy to the unamplified pulse energy measured to give a value of the gain for each size of amplifier. The small signal gain levels obtained from these tests will be fed back into the models for the 10PW Facility to ensure the model is a true representation of the facility.

Disc Amplifier Chain

Numerous amplifier combinations have been modelled for the disc amplifier chain. This modelling based on the Frantz-Nodvik method [5] considers gain components and passive components as well as active isolation components. By taking the gains and losses and the beam size into account it is possible to model the energy at each stage within the system being considered. To ensure that the model is accurate it has been tested by modelling the existing Vulcan beam line. The model has been shown to be good to within a few percent under these tests. With the characteristics already modelled it is possible to take a further step and calculate the breakdown integral, or B-integral [6], for these systems. Although it is possible to operate a long pulse laser system with a B-integral value of 7, when aiming to deliver in excess of 1 kilojoule it is advisable to keep it as low as possible. It was decided to ensure the B-integral of the Long Pulse Pump Laser was at most 3, with a target value of 2. The key characteristics of the most likely designs being considered are shown in Table 2.

From the modelling conducted and reported in table 2 above two designs came to the fore, options A and B, as both designs reduced the number of capacitor bank circuits required and kept the maximum fluence levels lower. As an added advantage option B allows for reuse of some equipment already made available to the project. Therefore option B was selected for further consideration.

Laser Architecture

Following the rod amplifier chain the energy will be increased in a series of disc amplifiers, as seen in figure 5, with increases in aperture and divisions in the wavefront to keep it from exceeding the laser damage threshold for the components. After leaving the end of the rod chain a variable split will be introduced to enable control of the amount of energy being sent to each of the two amplifier chains. The beam will then increase in size from 45 mm diameter to 96 mm diameter leading to a reduction in energy density from 0.89 J/cm^2 to 0.14

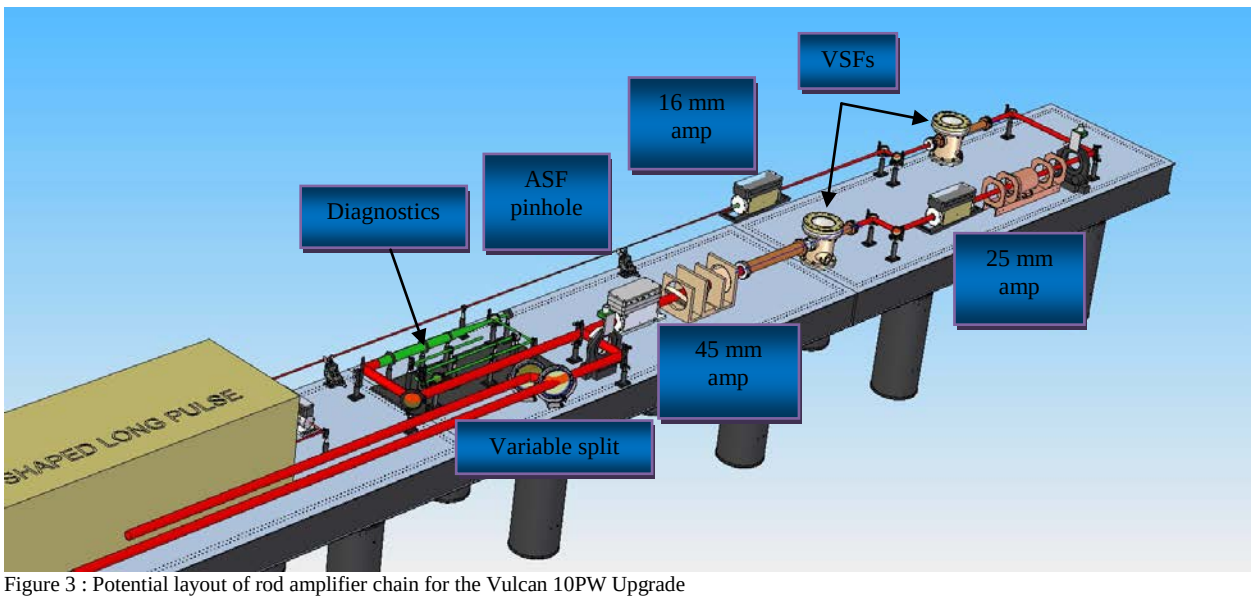

Figure 3 : Potential layout of rod amplifier chain for the Vulcan 10PW Upgrade

Option	Description	System I/P (mJ)	Corner Energy (J)	Output of 208 Energy (J)	Highest fluence (J/cm^2)	B-Integral
	System design limits	2	15	1500	5	3
A	After rod chain 2 way split, double passed 108, Apodiser, 4x double passed SQ 208s	0.200	1.07	1316	4.06 O/p 208s	0.84
B	After rod chain 2 way split, double passed 108, Apodiser, 2x double passed circ (sq beam) 208s, 2x single passes SQ 208s	0.304	9.14	1248	3.85 O/p 208s	1.78

Table 2 : Leading options considered for the disc amplifier chain layout and the limits within which the designs were judged

J/cm^2.

At this point the beam will enter a double passed 108 amplifier arrangement of a plate polariser, Faraday rotator, disc amplifier and retro reflector which will be used to boost the energy of the beam by a factor of ~50. The beam will pass through the polariser before arriving at the Faraday which will rotate the polarisation by 45 degrees when activated. The amplifier will be orientated at 45 degrees to match the polarisation change. After being amplified in the first pass the beam will be reflected back along a similar path and amplified further in the second pass. The polarisation will be rotated a further 45 degrees through the Faraday such that at the polariser the beam is rejected from the surface.

During the transit from the double passed 108 amplifier system to the '3 way VSF' the polarisation of the beam will be rotated back to horizontal. The beam will be apodised to a square prior to entering the '3 way VSF'. The energy at this point will be about 76 J post apodisation.

A design incorporating four double passed amplifiers has been considered, but rejected as it would require 24 rectangular discs. The first two 208 amplifiers will use the existing 12 elliptical discs in double pass mode, but as the beam needs to be square through the final amplifier this beam will be 127x127 mm. This will then be followed by the final output 200 slab amplifiers which will be full aperture 180x180 mm beams.

To enable this architecture a three way VSF would be required where the two beams would be angularly multiplexed through two pinholes. A conceptual design is shown in figure 6. On the first pass the square beam is reflected off a small, 25 x 35 mm mirror to direct it into the first pinhole and through to the double passed elliptical disc amplifier. After being amplified the beam passes back into the VSF and through a second pinhole separated from the first by 20 mm and through to the output rectangular disc amplifiers. Passing off centre through the second lens of the 'three-way VSF' introduces errors to the beam, but modelling indicates the errors are less than λ/10 in a double pass configuration.

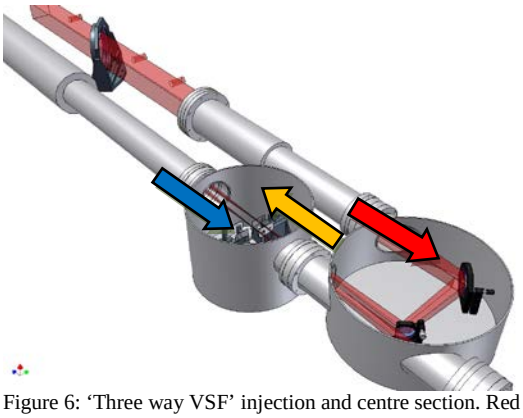

Figure 6: 'Three way VSF' injection and centre section. Red arrow – beam injection. Orange arrow – first pass through pinhole heading towards double pass 208 amp. Blue arrow – return from double passed 208 amplifier passing through second pinhole on way to 200 slab amplifier.

The major challenge with this design is the required Laser Damage Threshold of the 25 x 35 mm mirror in the VSF which is required to withstand 10.5 J/cm^2. Recent discussions indicate that the risk associated with this optic has been reduced as

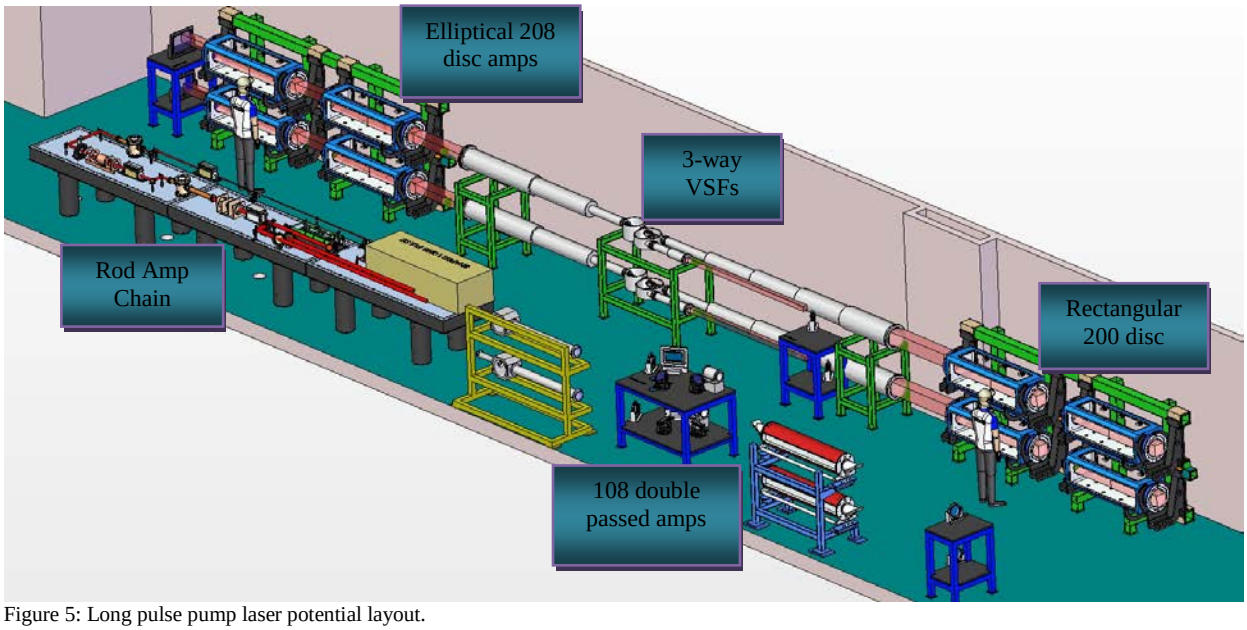

Figure 5: Long pulse pump laser potential layout.

Amplifier	Energy at output	Fluence at output
Input of 108 amplifier	2.4 J	38 mJ/cm^2
Output of 108 amplifier	123 J	1.94 J/cm^2
After apodiser	76 J	1.8 J/cm2
Output of 208 double pass amplifier	506 J	3.1 J/cm^2
Output of 208 rectangular amplifier	1247 J	3.9 J/cm^2

Table 3: Energies and fluences throughout the disc amplifier chain.

optics developed for the Laser MegaJoule Project [7] are designed to withstand in excess of 40 J/cm^2 at similar pulse lengths. Samples are being obtained to confirm the Laser Induced Damage threshold.

After full amplification each beam would have in excess of 1.2 kJ in a 3 ns flat topped pulse as per the initial specification. The key characteristics are shown in Table 3 above.

The disc amplifiers and Faraday isolators from the Disc amplifier chain will be powered from a new capacitor bank [8].

From experience of the Vulcan Laser System which has energy stability 95% of shot requests being delivered to within +/- 20% of the requested energy, it is anticipated to have a similar energy stability with the 10PW Project. Most of the issues affecting this stability are related to the stability of the alignment of the beam between the oscillator and the end of the rod chain. It is anticipated that this energy stability will be improved for the 10PW Facility by better diagnostics and alignment procedures for the rod chain. It could be further improved by the use of an automated alignment system which would adjust the alignment of the rod amplifier chain prior to the shot – to be effective this would require more diagnostics.

MIRO modelling of the Amplifier Chain

Understanding the performance of the proposed laser chain is important to predict the required input energy to give the expected output pulse energy, fluence throughout the amplifier chain and the temporal pulse shape.

The analytical program MIRO [9] was developed to simulate propagation and amplification of laser beams in Nd:glass laser systems. The physical effects which MIRO takes into account are: saturated amplification, absorption, Kerr effect, birefringence and aberration.

The rod amplifier chain, being based on the Vulcan rod amplifier chain, is fairly well understood. Tests on the Vulcan rod chain have proven the MIRO model up to the end of the rod chain. This said the ongoing gain test measurements of the Quantel rod amplifier will provide essential data for the modelling of the new system. Further experience of running the Vulcan Shaped Long Pulse Oscillator in conjunction with the Vulcan Rod Amplifier chain will give further confidence that the rod chain and SLP required for 10PW Long Pulse Pump Laser is well understood.

A model of the proposed amplifier chain has been developed which agrees well with Frantz-Nodvik [6] calculations for the saturated amplification of this system. As a further test both these methods have been used to model the Vulcan rod and disc amplifier chain where both gave good correlation with each other and the Vulcan system performance. Table 4 shows the MIRO model calculated system gains and energies at key points.

Using the amplifier chain models developed with MIRO it is possible to predict the change in the temporal pulse shape as it passes through and off the many optical components in a laser amplifier chain. It is possible to set an output characteristic such as temporal pulse shape and use the MIRO models to predict the input pulse shape required to give the required output pulse shape. This was originally anticipated to be a 3 ns square, or top hat, pulse for maximum energy extraction. However a sharp temporal cut off in the square pulse transfers to the spectrum of the amplified seed pulse due to the seed being a chirped pulse. Sharp changes in wavelength such as this can lead to a degradation in contrast, see OPCPA chapter. A pulse shape will need to be selected which compromises between maximum energy extraction and high contrast, which will probably be closer to a 3ns super Gaussian pulse. To anticipate the change in pulse shape as the pulse is amplified through the amplifier chain the model needs to take into account the dominant effect of 'gain saturation' where pulse shapes are changed as the leading edge of a laser pulse achieves significantly higher gain than the trailing edge as it passes through the gain medium. The majority of temporal pulse shape distortion is predicted to occur within the disc amplifier chain where the amplifiers are running in the saturated mode. The model has been developed using analytical expressions for the input pulse shape, defined in both spatial and temporal terms, and using an 'equivalent' optical chain modelled in MIRO to that envisaged (using Direct 3D geometrical optics) before a 50% split. The input temporal profile can be adjusted to give the best flat topped pulse possible at the output.

The diagnostics for the 10PW Long Pulse Pump Laser system will be similar to the beamline diagnostics in the existing Vulcan system.

OPCPA booster stage pumping options

As part of the design of the OPCPA Amplifier Stages [10] one scheme requires a pre-amplification stage to be considered, this would require ~15J in a 50x50 mm beam at 527 nm to pump it. A number of options are being considered including obtaining this booster stage pump from various positions in the Long Pulse Pump Laser chain.

Option 9a has a requirement for a double passed rod amplifier,

	Beam size	Single pass gain	Energy
SLP Output	3.6 mm dia		56 uJ
9 mm rod amp	3.6 mm dia	18	
16 mm rod amp	10.6 mm dia	25	
25 mm rod amp	18 mm dia	16	
45 mm rod amp	36 mm dia	5.5	5J
Splitter for 2 beams	36 mm dia	Single pass Gain per amplifier	2.4 J
Double pass 108 disc amplifier	90 mm diameter	10.5	101J
Double pass 2x elliptical 208 disc amplifier	127 mm x 127mm	2.1	475J
Single pass 2x Square 208 disc amplifier	180 mm x 180mm	2.1	1260 J

Table 4: data obtained from the MIRO model of the proposed 10PW Facility

probably a 45mm rod, which has not been included as part of the original project. Option 9b removes a lot of energy from the system resulting in working the front end and rod chain harder to compensate. As the double passed 108 amplifier system contains polarisers, which in Vulcan are the Long Pulse 'fuse' (lowest damage threshold component) for the system, this is inadvisable.
Therefore from a system point of view it is preferable to remove the OPCPA booster stage pump beam either at the output of the 208 amplifiers or after the beam has been frequency doubled to 527 nm, where the percentages of the beam extracted are significantly lower. From an OPCPA viewpoint, it would be preferable to extract the pump at the end of the rod chain, where pulses would be available every two minutes.
The temporal pulse shape distortion of this Booster stage pump would not have an identical pulse shape to the main beam if taken from the end of the rod chain. After amplification in a double passed rod it would have a more rounded shaped pulse compared to the stage 1 and 2 pulses, assuming a saturated gain from an additional rod amplifier. Modelling shows that this would not be a significant issue for the OPCPA Booster stage

Conclusions

A design has been modeled and assessed both using Frantz-Nodvik and MIRO software. This design has been deemed suitable for delivering 600 J at 527 nm in a 3 ns pulse to the OPCPA Stages of the Vulcan 10PW Upgrade.

References

1. 10PW Facility
2. OPCPA Process
3. Development, commissioning and experimental delivery of full energy shaped long pulse laser pulses on Vulcan. CLF Annual report 2008-2009 pp 283-285.
4. Quantel SA, 2 bis Avenue du Pacifique, BP23 91 941, Les Ulis CEDEX, France
5. L.M. Frantz and J.S. Nodvik, J. Appl. Phys. **34** (1963), p. 2346.
6. High-Peak-Power Nd:Glass Laser Systems, D.C. Brown, Springer series in Optical Sciences, ISBN 3-540-10516-6
7. High-gain direct-drive laser fusion with indirect drive beam layout of Laser Mégajoule, B. Canaud, Nuclear Fusion, Vol 47, No.12, 1652
8. Cap Bank Design CLF Annual Report 2011
9. Olivier Morice : Miró: Complete modeling and software for pulse amplification and propagation in high-power laser systems", Optical Engineering- June 2003 - Volume 42, Issue 6, pp. 1530-1541 a2930_1
10. OPCPA Stages, CLF Annual Report 2011

Option	Split position	%age split	SLP o/p	Booster pump o/p	System B-integral	Highest fluence	Pos'n of highest fluence
a	Rod chain	23%	6.88E-5 J	15.04 J	1.585	3.82 J/cm^2	O/p 208s
b	After DR	29%	8.82E-5 J	15.02 J	1.719	3.84 J/cm^2	O/p 208s
c	After 208	2.5%	5.72E-5 J	15.06 J	1.601	3.92 J/cm^2	O/p 208s
d	After Xtal	2.7%	5.78E-5 J	15.29 J	1.616	3.93 J/cm^2	O/p 208s

Table 5: An analysis of the options for pumping the OPCPA booster stage

Rectangular Slab Amplifier Development

Contact *Trevor.Winstone@stfc.ac.uk*

TB Winstone, AJ Frackiewicz, SEJ Chapman, DA Pepler, S Hancock, S Blake, C Hernandez-Gomez

Central Laser Facility
STFC Rutherford Appleton Laboratory, Chilton, Didcot, Oxon. OX11 0QX

Introduction

Laser discs have been the mainstay of high energy glass laser systems for the last 35 years. The traditional monolithically, or pour, clad discs are being phased out by manufacturers as processes developed for the National Ignition Facility (NIF)[1] and Laser MegaJoule (LMJ)[2] prove to have a higher yield of higher quality discs. This paper covers the Vulcan system implementation of design changes to elliptical disc amplifiers to take rectangular slabs.

Amplifier modifications

The disc amplifiers currently used in Vulcan are either a CLF design (Size 108mm and 150mm clear aperture) or amplifiers obtained from the Nova laser [3] (size 208mm clear aperture). The 208 Nova disc amplifiers were modified to use 8 flashlamps to pump the active laser glass, thus using half the number of capacitor bank circuits. These amplifiers have been operating successfully for 9 years within the Vulcan Petawatt facility[4]. As these types of amplifiers are well understood these will also be used in the design of the Vulcan 10PW Facility.

The Vulcan 10PW Upgrade Long Pulse Pump Laser design[5] has access to four of the Nova style 208 amplifiers not currently in use that are being made available to the project. As this number of amplifiers is insufficient we require additional amplifiers. For the final stage of amplification, the amplifiers will be built using rectangular Nd:glass slabs, which will require the development of new amplifier designs.

Traditionally the manufacture of laser discs has required a cladding material to be poured at high temperature around the hot Nd:doped laser glass and cooled over several weeks to room temperature. This cladding material is required to absorb Amplified Spontaneous Emission (ASE) within the plane of the disc and hence significantly reduce depletion of the energy stored in the disc. The monolithic, or poured, cladding process leads to a significant number of failures primarily due to stresses induced between the two materials. To dramatically improve yield a glue cladding process [6] was developed at Lawrence Livermore National Laboratory (LLNL).

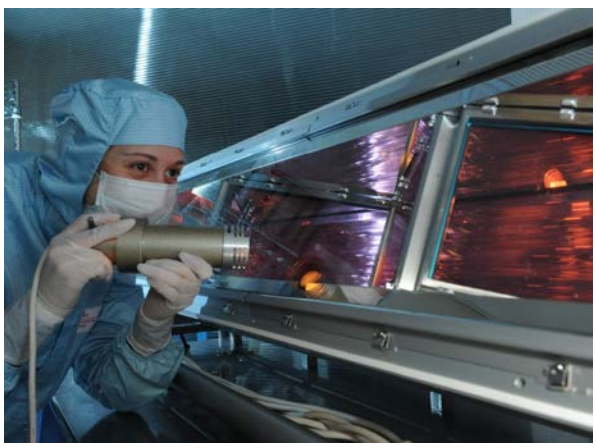

Figure 1: Inspection of 150 Rectangular slab amplifier

A design has been implemented to modify the 208 amplifier to take similarly sized rectangular glue clad slabs, referred to hereafter as 200 slabs. These slabs have been cut from material supplied by LLNL and clad with copper doped glass to absorb parasitic oscillations in the plane of the slabs.

Tests have been conducted on a 150 size slab amplifier (see figure 1) and a 200 size slab amplifier. The gain test of the 200 amplifier has concluded that it has a similar small signal gain to the 208 elliptical disc amplifier, the former giving 2.06 (at 1.8 kV) with the later 2.15 (at 1.9 kV), see figure 2.

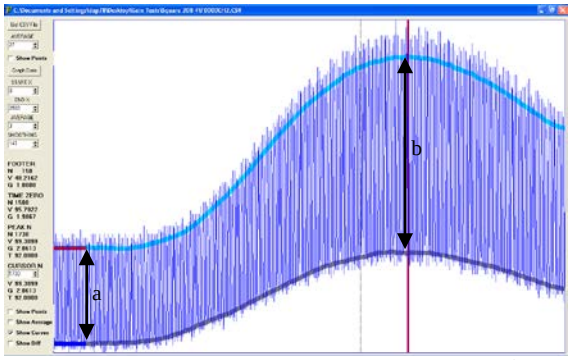

Figure 2: Gain test results showing Rectangular slab gain of 2.06 at 1.8 kV. Gain given by height at 'b' divided by height at 'a'.

Tests will also be conducted to assess the effect of firing the disc amplifiers at a repetition rate higher than the one shot per 20-30 minutes. This is limited by the thermal effects which are induced in the gain medium from the firing of the flashlamps. Although the flashlamps are cooled to remove as much heat as possible it is inevitable some heat will pass to the laser discs in the form of IR radiation. Currently the disc cavity is purged with Nitrogen, but not cooled. We are considering the option of cooling the cavity with the aim of trying to fire the amplifiers at one shot per 15 minutes for the task of near-field pumping of the OPCPA crystals in the 10PW Project.

Conclusions

Amplifiers of similar beam size, but using rectangular Nd:doped slabs have been built and tested at the Central Laser Facility to prove similar operational characteristics to the existing amplifiers. This has been essential to the continued operation of the Vulcan Laser System as well as the Vulcan 10PW Upgrade. Further modifications are being considered to fire the amplifiers at a higher repetition rate.

References

1. National Ignition Facility laser performance Status, Applied Optics, Vol. 46, Issue 16, pp. 3276-3303 (2007)
2. High Gain Direct drive fusion with indirect drive beam layout of Laser Megajoule, B.Canaud, Nuclear Fusion, Vol 47, No. 12, 1652
3. Present and future performance of the Nova laser system, JT Hunt, DR Speck, Optical Engineering, Vol 28:4, Apr 1989
4. Vulcan Petawatt - an ultra-high-intensity interaction facility, C.N. Danson *et al* 2004 *Nucl. Fusion* **44** S239
5. Vulcan 10PW Project: Design of the Long Pulse Pump Laser Design, CLF Annual Report 2010-11

6. PE Miller et al, Phosphate laser glass for NIF: production status, slab selection, and recent technical advances Proceedings Vol. 5341, Optical Engineering at the Lawrence Livermore National Laboratory II: The National Ignition Facility, pp.102-113

Vulcan 10PW Upgrade: Development of metallic 900 lines/mm pulse compression gratings

Contact *Trevor.Winstone@stfc.ac.uk*

TB Winstone, IN Ross, M Galimberti, A Lyachev,

C Hernandez-Gomez

Central Laser Facility
STFC Rutherford Appleton Laboratory, Chilton, Didcot, Oxon. OX11 0QX

D Smith, M McCullough

Plymouth Grating Laboratory
5, Commerce Way, Carver, MA 02330, USA

Introduction

The principle aim of the Vulcan 10PW project is to deliver a 30fs pulse with 300J of energy to target. The compressor design began by demonstrating that it was possible to compress high energy broadband pulses to 30fs using new grating technology

Previous development work

A programme of broad bandwidth diffraction grating development and measurement has been established to meet the stringent requirements of the Vulcan 10PW laser system. Gratings are strongly limiting items in large CPA systems as a result of their high cost, limited and ageing efficiency and modest damage threshold. Traditional gratings have been based on metallised photoresist holographic gratings which require fluences less than 0.2J/cm^2 and have 4 bounce efficiencies of typically 70% or less and consequently require very large beam and optics diameters and increased energy designs for the laser. Modest improvements can lead to significant increases in laser performance to target. These are holographic gratings photo-lithographically etched into photoresist and metallically over-coated. Figure 1 shows the simulated efficiency curve for an optimised square profile gold grating and indicates excellent efficiency and bandwidth. A number of possible developments have been discussed in literature, primarily concentrating on improving the damage threshold of conventional gratings and on the use of high damage threshold dielectric materials to either enhance the performance of the metallic gratings or even to eliminate the use of metals entirely. For the Vulcan 10PW laser we have investigated possible improvements for a wavelength range of up to 200nm centred at 910nm and for geometries and grating groove densities compatible with the re-compression of 3ns pulses. Initial tests[1] showed that gratings at line densities of 900 l/mm, 1000 l/mm and 1100 l/mm and ‘s’ polarization were rapidly approaching the simulated diffraction efficiency levels in house modeling had predicted. However the

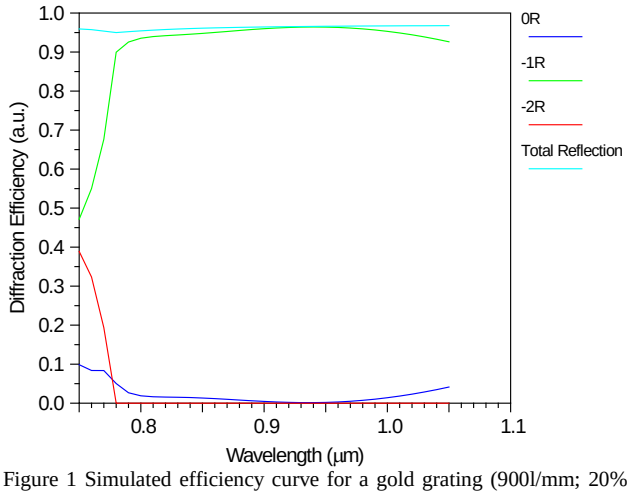

Figure 1 Simulated efficiency curve for a gold grating (900l/mm; 20% duty cycle; 370nm depth)

900 l/mm grating had shown maximum efficiency, so were chosen to take forward. Tests were then undertaken to compare silver coatings and gold coatings. Both of these were shown to be performing similarly.

Metallic Gratings improvements

Two possible improvements over the diffraction efficiency and laser damage threshold levels for the metallic gratings have been proposed.

a) Increase in the thickness of the metal layer to perhaps 200nm has been shown to yield higher damage threshold although this may lead to a reduction in the conformity of the profile to the ideal and hence to a reduction in efficiency and bandwidth.

b) As the presence of the photoresist contributes to the low damage threshold and is not easy to coat with good uniformity, an improved performance may be achieved by reactive ion etching the resist profile into the substrate and eliminating the photoresist prior to applying the metal coating.

Metallic grating development: Diffraction efficiency and laser damage threshold results

The compressor gratings must satisfy a number of criteria as explained in the earlier section. The grating must have low line density, ideally ~ 900 l/mm, and must have good diffraction efficiency at 900nm over the required bandwidth. They will handle large diameter beams > 0.6 m containing large energy ~500J, therefore they must have a laser damage threshold(LDT) that allows for a safety margin to be able to operate at half of the damage threshold i.e. LDT of 160 mJ/cm2 to operate regularly at 80 mJ/cm2.

The theoretical calculations showed that the best efficiency is obtained when operating the gratings at Littrow angle with an off-plane configuration at ‘s’ polarisation as described above.

In our earlier report [1] we tested several samples of silver and gold gratings at 900 l/mm of binary profile. The tests showed that both silver and gold gratings of the binary type operating at Littrow out of plane configuration have quite uniform diffraction efficiency above 90% across the required bandwidth. Experience in Manufacture has led Plymouth Gratings to more regularly hit the best diffraction efficiency across the full operation bandwidth of the 10PW Project. In figure 2 the diffraction efficiency achieved for 900 l/mm Binary type Ag coated fused silica samples in Littrow (24 degrees) out of plane (6.5 degrees) configuration at ‘s’ polarization is shown. It clearly demonstrates that the diffraction efficiency is over 90 % and is uniform within the required spectral range, with uniform spatial diffraction efficiency. Figure 3 shows the diffraction efficiency achieved for 900 l/mm binary type gold grating samples in the same configuration.

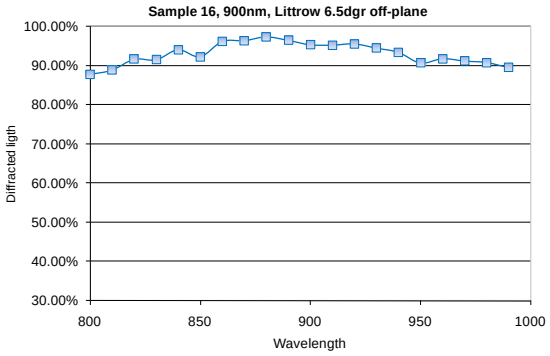

Figure 2 Diffraction efficiency for Grating sample # 16, Ag, 2'', FS, Binary Type, S – polarization

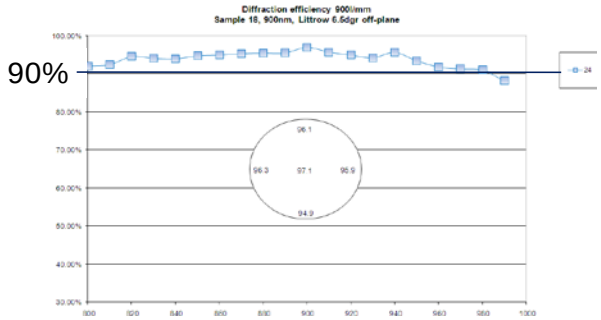

Figure 3 Grating sample # 18, 200 nm Gold on Photoresist, 2'', FS, Binary Type,

The fluence on the surface of the first compressor grating is 125 mJ/cm^2 and on the last grating 85 mJ/cm^2. For the last grating, where the pulse length will be 30 fs, the specification for the damage threshold has to ideally include at least a factor of two for safe operations, this means that the target specification is 170mJ/cm^2 for the final grating measured on the grating's surface**.** It was therefore important to confirm the laser damage threshold (LDT) for the new metallic grating samples for short pulse operation. Initial tests were conducted on the Astra facility and all subsequent tests have been conducted at *Vilnius University Laser Research Center(VULRC).* All samples were tested using a 45fs pulse at 's' polarisation with a centre wavelength of 800nm at 10 Hz, both in air and in vacuum.

The normal process is to test the grating samples for diffraction efficiency and then for LDT, table 1 shows a summary of the LDT for the gold and silver binary sample gratings manufactured with different parameters, this table shows that metallic gratings can be manufactured with the required target of 170 mJ/ cm^2. This shows a 50% uplift in LDT results from the initial batches due to ability to manufacture the gratings more reliably, improved cleaning techniques, and the variation of metal coating thickness. Figures 4a and 4b show the data obtained in the LDT tests for the best two samples. The ability to etch the grating reduces the impact of a further variable in the uniformity of the photoresist. The next step will be to produce

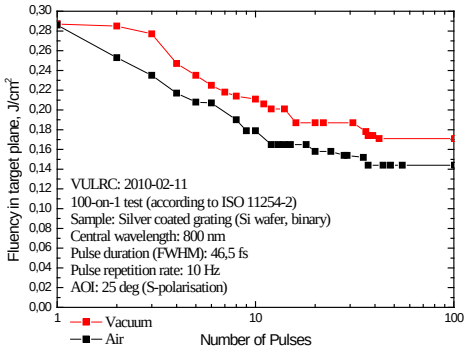

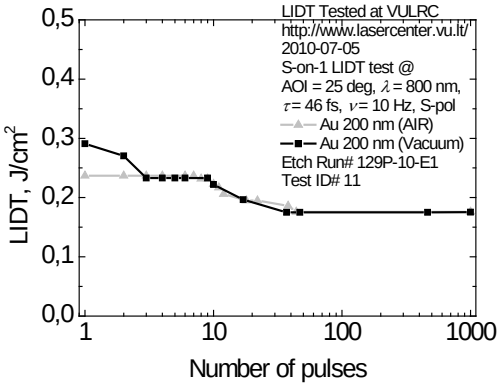

Figure 4a LDT results for silver coated binary 900l/mm gratings sample 15/batch3 . Figure 4b LDT results for gold coated binary 900l/mm gratings sample/ 11Batch 4

a medium size grating to confirm the performance achieved for the smaller samples.

Conclusions

This process of reducing the risks to the project by targeted development of grating technology at 900 lines/mm has been highly successful delivering samples capable of delivering excellent diffraction efficiency across the required bandwidth whilst withstanding the specified laser damage threshold suitable for operations.

References

1. Evaluation of new gratings for the Vulcan 10PW OPCPA Upgrade project, A.Lyachev et al, CLF Annual Report 2008/09.

Batch / Sample	Type of substrate	Coating	Line density	Angle of incidence	VACUUM: LIDT At 100 shots 40 fs, Vacuum, 800nm, 10 Hz
Batch3/16	FS substrates	Silver 100nm	900	25	0.162 J/cm2
Batch3/15	Si wafer	Silver 100nm	900	25	0.171 J/cm^2
Batch5/5	FS substrates	Silver 200nm	900	25	0.170 J/cm^2
Batch 4/9	FS substrates	Gold 200nm	900	25	0.170 J/cm^2
Batch 4/11	FS substrates	Gold 200nm/ etched	900	25	0.180 J/cm^2

Table 1. Summary of the optimum LDT tests obtained of different metallic gratings.

Pre-pulse generator for controllable picoseconds pre-pulses in TAP

Contact *ian.musgrave@stfc.ac.uk*

Ian Musgrave

Central Laser Facility, STFC, Rutherford Appleton Laboratory, HSIC, Oxfordshire, OX 11 0QX, UK

Introduction

In this contribution we discuss the optical arrangement used to generate controllable picoseconds pre-pulses in TAP. The development of this has been driven by the work of Robinson *et al* [1] where two laser pulses are used to reduce the fast electron beam divergence. With the development of the picosecond OPCPA pre-amplifier [2], there is sufficient seed energy to enable a relatively high loss system to be employed without degrading the performance of TAP.

Operation of the Pre-pulse generator

The pre-pulse generator is positioned between the output of the picosecond OPCPA pre-amplifier and the TAP stretcher. The schematic for the optical arrangement of the pre-pulser is shown in figure 1. The input pulse is incident on a half-waveplate and polarizing beam splitter (PBS) the relative orientation of these controls the ratio of the pre-pulse to main pulse intensity. The main pulse goes through the PBS and is incident on a roof prism that displaces the pulse horizontally, a steering mirror is then placed before a non-polarizing beam splitter (NPBS) to enable alignment into the TAP stretcher. The pre-pulse is reflected off the PBS and is also incident on a roof prism and is equally displaced horizontally. This roof prism is mounted on a translation stage with a micrometer to enable translation in steps of 0.5ps equating to adjustments of 75μm. A half-wave plate is then used to rotate the polarization of the pre-pulse to match that of the main pulse. A steering mirror and the NPBS are then used to match the propagation of the pre-pulse to the main pulse.

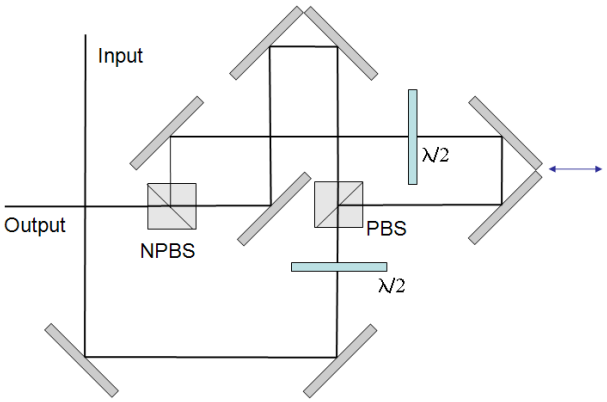

Figure 1. Schematic of the optical arrangement for the picoseconds pre-pulse generator showing the half-waveplates (λ/2), polarizing beam splitter (PBS) and non-polarizing beam splitter (NPBS).

Alignment and Calibration

The pre-pulser was aligned using the output from the TAP oscillator which produces pulses with ~150fs duration at 80MHz. The optical alignment was confirmed using the near and far-field monitors for the TAP stretcher. Temporal alignment was then achieved by introducing a slight tilt to the beam which introduces fringes to the beam in the near-field which are only visible when the pulses are temporally and spatially overlapped. In this way the nominal zero delay position was defined.

The calibration of the relationship between the relative ratio of pre-pulse to main pulse and the angle of the first half wave-plate was achieved using the oscillator and a power meter. It was found that the ratio of the pre-pulse to main pulse intensity could be adjusted from 1:1 to 1:25 in a controllable and repeatable fashion. The throughput of the device was also measured with the combined output of the main and pre-pulses being 40% of the input beam.

Operation

The picosecond pre-pulse generator was used during the experimental campaign in TAP in September 2010. An example of one of the autocorrelation traces recorded during that campaign is shown in figure 2. The settings for this target shot were for a separation of 4ps and a ratio of 1:10. Due to the symmetrical nature of the autocorrelation function a pre-pulse also generates a post-pulse. It is still linear though in that a separation of 4ps in time should be measured as 4ps and the relative ratios should still be the same in the autocorrelator. The lineout in figure 2 shows that the central peak is saturated but the separation of the main peak to the satellite peaks is equivalent to a separation of ~3.85ps.

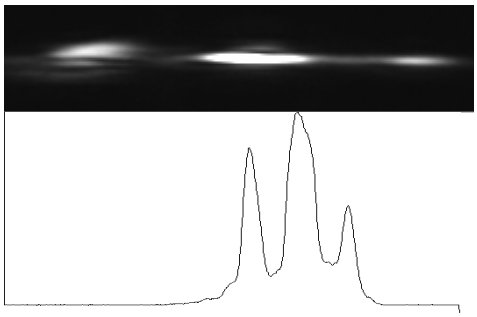

Figure 2. Autocorrelation and respective lineout for a target shot during the TAP campaign in September 2010.

Conclusions

In conclusion we present a simple device that enables the generation of controlled pre-pulses on the picoseconds time domain. This device was successfully used in the experimental campaign in TAP in September 2010.

References

1. A.P.L. Robinson, M. Sherlock, and P.A. Norreys, Phys. Rev. Lett. **100**, 025002 (2008).
2. I. Musgrave et al., Appl. Opt. **49**, 6558 (2010)